Black Hole to White Hole Quantum Tunnelling

by

Kate Clements

A thesis
presented to the University of Waterloo
in fulfillment of the
thesis requirement for the degree of
Master of Mathematics
in
Applied Mathematics

Waterloo, Ontario, Canada, 2019

I hereby declare that I am the sole author of this thesis. This is a true copy of the thesis, including any required final revisions, as accepted by my examiners.

I understand that my thesis may be made electronically available to the public.

Abstract

In this thesis, we explore the proposal that near the end of its lifetime, a Schwarzschild black hole will undergo a quantum transition into a 'white hole': an object which is precisely the time-reversal of the black hole. This transition takes the form of quantum tunnelling. In order to evaluate the tunnelling amplitude, we characterize the region where quantum gravity effects dominate as enclosed by intersecting hypersurfaces on which the trace of the extrinsic curvature is equal to zero. This allows us to recover the tunnelling amplitude as specified by the boost angle between the normals to these hypersurfaces. The long-term aim of this work is to find the complex solutions to the vacuum Einstein equations in the quantum gravity region, and thus provide a complete explanation for what happens to a black hole after it evaporates.

Acknowledgements

I would like to thank my supervisors Maïté Dupuis and Florian Girelli for their endless support throughout this Masters research project. I would also like to thank Hal Haggard and Abdulmajid Osumanu, without whose invaluable input this thesis would not have been possible.

Table of Contents

List of Figures

Chapter 1

Introduction & Background

1.1 Black Holes and White Holes

What happens to a black hole after it evaporates is a long-standing question. Classical general relativity predicts that at the centre of a black hole, there is a singularity where space and time end. This prediction is unrealistic, because it fails to take into account the quantum effects that dominate when gravity becomes very strong. It is well-known that a black hole's mass decreases with the passage of time via Hawking radiation [48, 49]. Hawking's description of black hole evaporation is based on quantum field theory in curved spacetime; it utilises a mean-field approximation that breaks down before the mass of the black hole reaches the Planck scale ($m_{Pl} = \sqrt{\hbar c/G} \approx 2.176 \times 10^{-8}$kg). We would like to investigate what happens to the black hole and the matter trapped inside it as we approach the Planck regime.

There are many theories concerning what happens to the matter that falls into a black hole. In this thesis, we explore the proposal that when the mass of a black hole reaches the Planck regime, it does not simply disappear; instead, it undergoes a quantum transition whereby the black hole horizon evolves into a white hole horizon. The possibility of a black-to-white hole transition was first proposed by John Lighton Synge in 1950 [82], and it has more recently been studied using loop quantum gravity techniques [7, 8]. In the quantum transition region, Einstein's general relativity is violated by quantum effects. The transition from black hole to white hole takes the form of quantum tunnelling, and we deduce an approximation for the tunnelling amplitude. After the tunnelling process occurs, the matter that was trapped inside the black hole can slowly escape. It has been suggested that the black-to-white hole transition could result in some observable astrophysical phenomena such as Fast Radio Bursts (FRBs) or high-energy cosmic rays [11, 12].

Our study has some limitations. In particular, although various authors [13, 76] have claimed that the black hole to white hole scenario offers a resolution to the information loss paradox, we do *not* expect our current work to solve the information loss problem. The reasons for this are:

- We do not consider the time-dependence of the black-to-white hole transition. Since

information loss is time-dependent, our static study will not provide any insight into what happens to the matter that falls into a black hole.

- We have not considered the evolution of the black hole before or after the quantum transition. If the evaporation and 'leaking out' processes are not sufficiently long compared to the time taken for the transition, it may not be appropriate to model black hole to white hole tunnelling as a static process.
- Studying the black hole to white hole transition does not explain what happens to the information that has fallen into the black hole during the Hawking evaporation process.
- We are only considering the tunnelling transition itself, and aiming to deduce the tunnelling amplitude. We are not proposing any mechanism by which the information that has fallen inside the black hole is allowed to leak out of the white hole after the transition occurs.

This thesis is organised as follows. In Chapter 1, we review the geometric properties of black and white holes, and discuss the regions of spacetime in which Einstein's general relativity is violated. We describe the black-to-white hole tunnelling proposal and consider the current state of knowledge regarding this topic. In Chapter 2 we introduce the spacetime we would like to study: the Schwarzschild black hole. We discuss the validity and usefulness of various coordinate systems used to describe the Schwarzschild black hole. Penrose diagrams are reviewed for the general Schwarzschild spacetime and for the black-to-white hole transition. Since the transition takes the form of quantum tunnelling, we revise the basics of quantum tunnelling in Chapter 3. We give a simple example of one-dimensional tunnelling through a rectangular potential barrier, and review the path integral formulation from which we obtain an expression for the coefficient of transmission for tunnelling. In Chapter 4 we begin to study the specifics of our chosen spacetime, and deduce its full gravitational action. We find that the action is dependent on the boost angle between the normal vectors to the surfaces characterizing the 'quantum gravity region' in which general relativity is violated. We calculate the geodesics defining these surfaces in Chapter 5, and use them to compute the boost angle in Chapter 6. We find that using the Kruskal coordinates yields a finite boost angle in the region close to and on the black hole horizon. We plot the boost angle in the interior region, the exterior region and on the horizon, and we consider the implications of these results for the probability of black-to-white hole quantum tunnelling. Finally, in Chapter 7 we consider the limitations of our calculations and identify interesting areas for future study.

1.1.1 What is a White Hole?

A white hole is the time-reversed version of a black hole. In a white hole, matter can only move outwards. White holes could represent the future of all black holes: various authors have proposed that after most of the black hole's mass has evaporated via Hawking radiation and it approaches the Planck mass, it quantum tunnels into a white hole from

which the matter that fell inside can 'bounce' out [13, 76]. This quantum transition is allowed since the laws of general relativity break down at the Planck scale and Einstein's equations are no longer valid.

From the outside, the geometry of a white hole is indistinguishable from that of a black hole [13]. The standard Schwarzschild line element with signature $(-,+,+,+)$ is

$$\mathrm{d}s^2 = -f(r)\mathrm{d}t^2 + f(r)^{-1}\mathrm{d}r^2 + r^2 d\Omega^2, \tag{1.1}$$

where r_s is the Schwarzschild radius $r_s = \frac{2GM}{c^2}$ for a black hole of mass M and we define $f(r) = 1 - \frac{r_s}{r}$. $d\Omega^2$ is the metric on a unit two-sphere [15]:

$$d\Omega^2 = d\theta^2 + \sin^2\theta d\phi^2. \tag{1.2}$$

When $r > r_s$, the line element in Equation 1.1 describes both the exterior of a black hole and the exterior of a white hole. The difference between black and white holes becomes apparent at the horizon $r = r_s$: the consequence of time reversal is that for a white hole the matter is outgoing rather than infalling as it was for the black hole. This means that the matter that fell inside is allowed to escape after the quantum transition occurs. Since the mass of the white hole is very small and its horizon is Planck size, we expect the matter to leak out very slowly; the white hole can thus be viewed as a long-lived remnant of the black hole [13].

1.1.2 Interior Geometry of a Black Hole

As the mass of a black hole decreases via Hawking radiation, its interior geometry is altered. The interior is composed of spacelike surfaces of topology $\mathcal{S} \times \mathbb{R}$ where $\mathcal{S}$ is a circle; i.e. it is a long cylinder. As time passes and the black hole evaporates, the length of the cylinder increases while its radius decreases (see Figure 1.1). It has been shown by Christodoulou and De Lorenzo [23] that although the area of the black hole's horizon will be very small near the end of its evaporation, the length of the cylinder will continue to increase linearly with time.

The age of a black hole is of no consequence to the *exterior* geometry. An old black hole that has evaporated to mass M has the same exterior geometry as a young black hole of the same mass [13]. However, the *interior* geometry of these two holes will be very different: the volume of the older black hole's interior will be much larger than that of the young hole.

1.1.3 Quantum Tunnelling from a Black Hole to a White Hole

As discussed above, the mass of a black hole decreases with time via Hawking radiation. When the mass approaches the Planck mass m_{Pl}, the strong distortion of spacetime geometry means that general relativity is no longer valid and Einstein's equations are violated for a brief interval of time [22, 25, 28, 45, 78]. During this interval, the causal structure

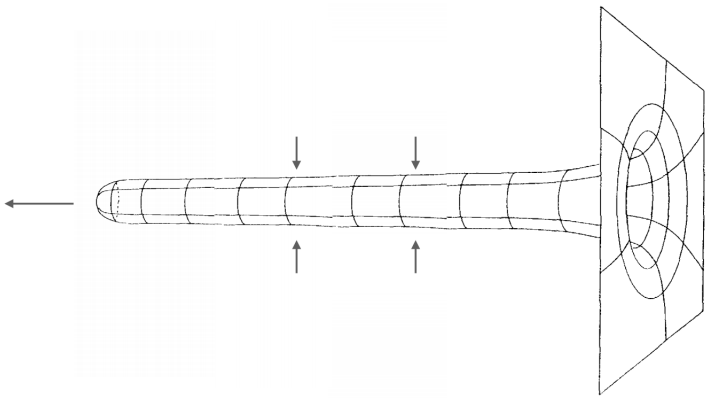

Figure 1.1: Interior geometry of an old black hole. As time passes, the length of the cylinder increases while its radius decreases. Diagram courtesy of [13].

predicted by classical general relativity is altered [35, 36, 51, 53, 62].

It was previously thought that black holes will eventually radiate away all their mass, and simply 'disappear'. In the words of Stephen Hawking, 'quantum theory will cause black holes to radiate and lose mass. It seems that they will eventually disappear completely, taking with them the information inside them' [47]. We no longer believe that this is the case. Instead of disappearing, the black hole will undergo a quantum transition into a white hole [4, 46, 63, 64]. This transition takes the form of quantum tunnelling. The information trapped inside can then slowly leak out, and the white hole might eventually disappear completely [40, 68].

The probability for a black hole to tunnel into a white hole is small until the black hole has evaporated so much so that its mass is of the order of the Planck mass, $m_{Pl} = \sqrt{\hbar c/G}$. This means that the tunnelling probability will not become significant until near the end of the evaporation process. The probability p scales the same way as the standard tunnelling factor:

$$p \sim e^{-S_E/\hbar} \tag{1.3}$$

where S_E is the Euclidean action. For a stationary black hole of mass m, we can approximate $S_E \sim Gm^2/c$ [13], so that

$$p \sim e^{-(m/m_{Pl})^2}. \tag{1.4}$$

It is clear from Equation 1.4 that as $m \to m_{Pl}$, the tunnelling probability becomes of order unity. This result has been derived more thoroughly by Christodoulou et al. in [22, 25].

There are two distinct regions of a Schwarzschild black hole in which quantum effects dominate and Einstein's general relativity alone is no longer sufficient to describe the physics. These are:

1. The central Schwarzschild singularity $r = 0$, where curvature becomes extremely large.

2. The tunnelling region near the horizon $r = r_s$, where the black hole undergoes a quantum transition into a white hole.

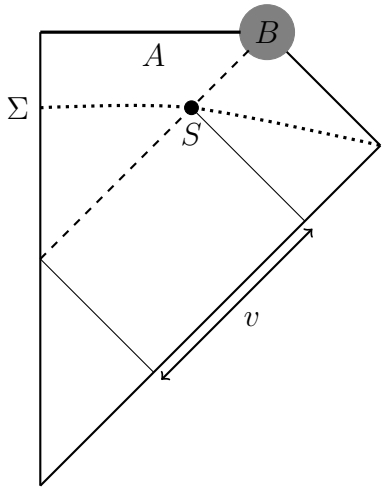

Figure 1.2: Penrose diagram of a classical black hole. The dashed line represents the black hole's horizon. The dotted line is a Cauchy surface Σ, and S is a two-dimensional sphere at the point at which the surface Σ crosses the horizon. A and B are the regions in which Einstein's general relativity is violated.

Following [13], we will refer to the regions corresponding to 1 and 2 as A and B. Figure 1.2 is a Penrose diagram of a classical black hole. The dashed line represents the horizon, and the dotted line is a Cauchy surface Σ that crosses the horizon at some time v. The section of Σ which is inside the horizon is denoted by Σ_i. We can fix Σ_i by considering a two-dimensional spacelike sphere S in four-dimensional Minkowski space. This sphere determines a preferred three-dimensional ball Σ_i bounded by S: the one with maximum volume. Choosing Σ_i to have maximal volume provides an invariant definition of the 'volume inside S' [13].

Region A is characterized by the large curvature of spacetime as we get close to the singularity at the centre of the black hole, and it is inclusive of the singularity. Region B is near the end of the evaporation: the area of the black hole horizon decreases until it reaches Region B. The quantum gravitational effects in A and B are distinct, and we must therefore consider the two regions separately.

Region A

The curvature of our spacetime increases as we move towards the singularity at the centre of the black hole, and the Schwarzschild radius r_s (which is a temporal coordinate inside the hole) decreases. When the curvature approaches Planckian values, quantum gravitational effects become significant and the laws of classical general relativity are no longer applicable [77, 88].

The interior geometry of an old black hole is a long cylinder (see Section 1.1.2). With the passage of time, its length increases and its radius decreases. The interior volume V scales as

$$V \sim m^4/\sqrt{\hbar}. \tag{1.5}$$

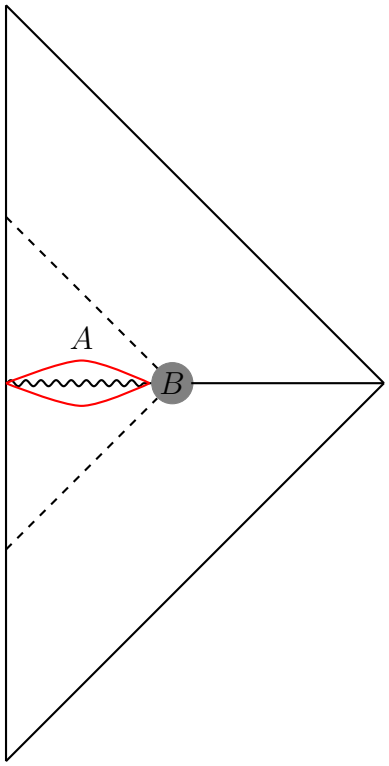

Figure 1.3: Spacetime diagram for a black-to-white hole transition. The dashed lines are the black hole horizon (below) and the white hole horizon (above). Regions A (enclosed by the red curves) and B are the regions in which general relativity is insufficient to describe the Schwarzschild black hole.

Bianchi et al. justified this result in [13]. In the classical limit $\hbar \to 0$ the interior volume of the black hole diverges with $V \to \infty$. In regions of high curvature where quantum gravitational effects become significant, V remains finite. When the radius of the cylinder reaches some minimal value, it 'bounces back': the radius begins to increase while the length decreases. We recognize this bounce as the quantum transition from a black hole to a white hole state. Analytic continuation of the Einstein equations across the singularity makes this transition possible.

Region B

For Region B, we are interested in quantum effects that occur when a sufficient amount of time has passed since the gravitational collapse. An upper bound for this time can be inferred from the Hawking radiation: $\sim m_0^3/\hbar$ where m_0 is the initial mass of the black hole [13]. It has previously been assumed that Hawking evaporation will continue after the curvature reaches Planckian values. We now believe this to be false, since the usual laws of general relativity are not valid at high curvature. Figure 1.3 is a spacetime diagram depicting a black-to-white hole transition. The dashed lines show the black hole horizon (below) and the white hole horizon (above). The high curvature region, Region A, is

represented by the area enclosed by the red curves. It has been shown in [28, 45] that the Einstein equations are satisfied everywhere on this spacetime except for the regions A and B, including the area between the black and white hole horizons (enclosed by the dashed lines in Figure 1.3). The quantum transition happens between these two horizons: the tunnelling process results in the black hole interior turning into a white hole interior of the same mass. The size of the white hole horizon is equal to that of the black hole, and is likely to be very small since we expect the black hole to approach the Planck mass before the probability of tunnelling becomes significant. The interior volume of the white hole will be very large, due to the elongation of the black hole's geometry during its evaporation. Its lifetime will be dependent on the age of the black hole, since the white hole's evolution is the time-reversed evolution of the black hole.

The time taken for the quantum transition has been calculated by Christodoulou and D'Ambrosio using a spinfoam model to be $\Delta\tau \sim m$ [22]. It was also shown in [22] that the probability of tunnelling per unit time, p, scales as

$$p \sim e^{-m^2/\hbar}, \tag{1.6}$$

where m is the mass of the black hole at the time of the tunnelling. As stated above, the time taken for the black hole to evaporate to Planckian mass is proportional to $m_0^3/\hbar$, and we can therefore say that the lifetime of the black hole

$$\tau_{bh} \sim m_0^3/\hbar \tag{1.7}$$

and

$$\Delta\tau \sim \sqrt{\hbar}, \tag{1.8}$$

which means that Region B is Planckian in size.

1.2 Counter-Proposal

As previously mentioned, the black-to-white hole tunnelling proposal is one of many theories concerning what happens to the matter that falls into a black hole. We now briefly consider a recent result from loop quantum gravity which suggests that the quantum bounce experienced by an old black hole does *not* in fact lead to the evolution of its horizon into a white hole horizon. Alesci et al. [2] propose an alternative model of the interior geometry of the Schwarzschild black hole, in which the transition to a white hole does not occur. This work builds on a previous study where an effective Hamiltonian constraint was derived for the Schwarzschild geometry starting from the full loop quantum gravity (LQG) Hamiltonian constraint [1]. The expectation value for this effective Hamiltonian constraint was computed for coherent states sharply peaked around a spherically symmetric geometry. The new constraint serves as a replacement for the Hamiltonian constraint of general relativity. In [2], the effective Hamiltonian constraint is used to study the interior region of the Schwarzschild black hole. The authors choose two different coherent states, and show that in each case the classical Schwarzschild singularity is replaced by a quantum bounce (as predicted by loop quantum cosmology [6,9]) followed by a homogeneous expanding universe

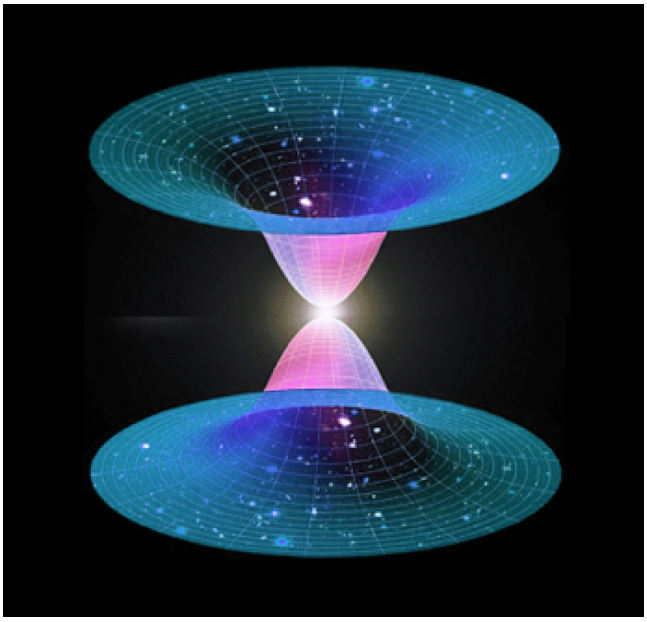

Figure 1.4: An artist's impression of a black-to-white hole transition. Image courtesy of [76].

with no evidence of the formation of a white hole horizon. Their effective description of the Schwarzschild interior geometry has the following properties:

- All dominant quantum gravity corrections in the full LQG theory are also present in the effective Hamiltonian H_{eff}.
- In the classical limit $\hbar \to 0$, H_{eff} reduces to the classical value predicted by general relativity.
- The effective metric is in accordance with the classical metric at low curvature, and diverges from it when the Planck scale is approached.

Alesci et al. show that for each choice of coherent state, the metric function $\Lambda(\tau)$ does not vanish at any time $\tau < 0$, which means that there is no formation of a white hole horizon after the quantum bounce. An advantage of this proposal is that it circumvents the large quantum effects that occur near the classical event horizon of the Schwarzschild black hole. However, it is limited by its dependence on the choice of coherent states.

1.3 Conclusion

In this chapter we introduced the proposal that we would like to study: a black hole approaching the Planck mass will quantum tunnel into a white hole from which the matter that was trapped inside can slowly leak out. We discussed the geometries of black and white holes and described the two regions of a black hole spacetime in which general relativity

fails. Finally we considered a recent counter-proposal to black-to-white hole tunnelling. In the next chapter we revise the Schwarzschild black hole, and explore various ways in which we can represent the black-to-white hole transition using spacetime diagrams.

Chapter 2

The Schwarzschild Black Hole

Recall that we would like to study the quantum transition from a black hole to a white hole in the context of the Schwarzschild black hole. In this chapter, we revise the Schwarzschild black hole and some of the many coordinate systems that may be used to describe it, and discuss the merits of using different coordinates. We expect the quantum transition to occur in the vicinity of the black hole horizon $r = r_s$ (this will be further discussed in Chapters 6 and 7) and it is therefore useful to work in a coordinate system that is well-defined at this point, such as the Kruskal coordinates.

2.1 The Schwarzschild Metric & Birkhoff's Theorem

The Schwarzschild solution is an exact and unique solution of Einstein's field equations in a vacuum. It may be used to describe any static and spherically symmetric object, including a black hole. In spherical coordinates $\{t, r, \theta, \phi\}$, the Schwarzschild metric is

$$\mathrm{d}s^2 = -\left(1 - \frac{r_s}{r}\right)\mathrm{d}t^2 + \left(1 - \frac{r_s}{r}\right)^{-1}\mathrm{d}r^2 + r^2\mathrm{d}\Omega^2 \tag{2.1}$$

where r_s is the Schwarzschild radius defined in Section 1.1.1 and $d\Omega^2 = d\theta^2 + \sin^2\theta d\phi^2$ is the metric on a unit 2-sphere. From now on we will use natural units such that $c = \hbar = G = 1$. In these units the Schwarzschild radius is $r_s = 2M$ where M is the mass of the black hole. If we let $f(r) = 1 - \frac{r_s}{r}$ as in Section 1.1.1, then

$$\mathrm{d}s^2 = -f(r)\mathrm{d}t^2 + f(r)^{-1}\mathrm{d}r^2 + r^2 d\Omega^2 \tag{2.2}$$

(Equation 1.1). The mass of the black hole M can be time-dependent, but the external spacetime described by the Schwarzschild metric must be static.

Birkhoff's theorem states that any spherically symmetric solution of Einstein's vacuum equations must be static and asymptotically flat. We must also be able to recover the Minkowski metric when $M \to 0$. This implies that the external spacetime of any such solution must be described by the Schwarzschild metric, Equation 2.1. An important

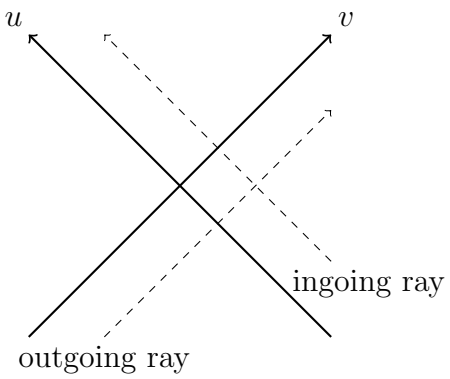

Figure 2.1: A spacetime diagram showing the (u, v) coordinates. Ingoing and outgoing massless particles or 'rays' are oriented at 45°.

consequence of Birkhoff's theorem is that a spherical mass distribution cannot emit gravitational waves [66]. The proof of this theorem is nontrivial and and we will therefore not cover it here: for a rigorous treatment, see *Hawking & Ellis* [48].

2.2 Kruskal Coordinates

It is clear from Equation 2.1 that the Schwarzschild metric in $\{t, r, \theta, \phi\}$ coordinates is not only singular at the centre of the black hole ($r = 0$), but also when $r = 2M$. The singularity at $r = 2M$ is a coordinate singularity, meaning that we may circumvent it by introducing a new coordinate system to describe the Schwarzschild spacetime. There are many choices we could make for these new coordinates, including those defined by Kruskal and Szekeres.

Consider massless particles that move radially in spacetime described by the Schwarzschild metric. The t and r coordinates will vary, but θ and ϕ are time-independent. We refer to particles for which r is decreasing as 'ingoing', and particles with increasing r as 'outgoing'. It can be easily shown (see for example [73]) that the ingoing particles move along curves with $v =$ constant and outgoing particles move along curves with $u =$ constant, where

$$v = t + r^* \tag{2.3a}$$

$$u = t - r^* \tag{2.3b}$$

$$\text{and } r^* = \int \frac{\mathrm{d}r}{1 - r_s/r} = r + r_s \ln \left| \frac{r}{r_s} - 1 \right|. \tag{2.3c}$$

v is called 'advanced time', and u is called 'retarded time'. As can be seen in Figure 2.1, the massless particles move along paths oriented at 45°, just as they would in flat Minkowski spacetime. This property makes the (u, v) coordinates ideal for describing radial null geodesics. Rewriting Equation 2.1 in terms of the (u, v) coordinates, we find that

$$\mathrm{d}s^2 = -\left(1 - \frac{2M}{r}\right) \mathrm{d}u\mathrm{d}v + r^2 \mathrm{d}\Omega^2. \tag{2.4}$$

r in the above equation is no longer a coordinate: it is merely used to define r^* in terms of u and v by

$$r^*(r) = \frac{1}{2}(v - u). \tag{2.5}$$

Substituting in $f(r) = 1 - \frac{r_s}{r}$, the metric can be recast in the form

$$\mathrm{d}s^2 = -f(r)\mathrm{d}u\mathrm{d}v + r^2\mathrm{d}\Omega^2. \tag{2.6}$$

The $r = r_s$ surface now occurs at $v - u = -\infty$, which is still a coordinate singularity. We would like to try and avoid this singularity. For this purpose, we consider the surfaces close to $r = r_s$, on which we can approximate

$$r^* \simeq r_s \ln\left|\frac{r}{r_s} - 1\right|. \tag{2.7}$$

Rearranging this equation gives

$$\begin{aligned} \frac{r^*}{r_s} &\simeq \ln\left|\frac{r}{r_s} - 1\right| \\ \Rightarrow e^{r^*/r_s} &\simeq \pm\left(\frac{r}{r_s} - 1\right) \\ \Rightarrow \frac{r}{r_s} &\simeq 1 \pm e^{r^*/r_s} \end{aligned} \tag{2.8}$$

where the upper and lower signs correspond to surfaces with $r > r_s$ and $r < r_s$ respectively. Using Equation 2.5, we can rewrite this as

$$\frac{r}{r_s} \simeq 1 \pm e^{(v-u)/2r_s}. \tag{2.9}$$

The function f may therefore be written as

$$f \simeq 1 - \left(1 \pm e^{(v-u)/2r_s}\right)^{-1}. \tag{2.10}$$

Since $v - u \to \infty$ when $r \to r_s$, we can approximate Equation 2.10 by its first-order Taylor expansion to give

$$f \simeq \pm e^{(v-u)/2r_s}. \tag{2.11}$$

The Schwarzschild metric can then be approximated by

$$\mathrm{d}s^2 \simeq \mp(e^{-u/2r_s}\mathrm{d}u)(e^{v/2r_s}\mathrm{d}v) + r^2\mathrm{d}\Omega^2. \tag{2.12}$$

We now introduce the null Kruskal coordinates U and V such that

$$U = \mp e^{-u/2r_s} \text{ and } V = e^{v/2r_s}. \tag{2.13}$$

We would like to use these new null coordinates to describe the entire spacetime. For this purpose, we first return to the exact expression for r^* (Equation 2.3c) and use it to express r as a function of U and V. Rearranging Equation 2.3c, we find

$$\begin{aligned}\frac{r^*}{r_s} - \frac{r}{r_s} &= \ln\left|\frac{r}{r_s} - 1\right| \\ \Rightarrow e^{r*/r_s} e^{-r/r_s} &= \pm\left(\frac{r}{r_s} - 1\right) \\ \Rightarrow e^{r^*/r_s} &= \pm e^{r/r_s}\left(\frac{r}{r_s} - 1\right). \end{aligned} \tag{2.14}$$

We know that $r^* = \frac{1}{2}(v - v)$, so

$$\begin{aligned} e^{r*/r_s} &= e^{\frac{1}{2}(v-u)/r_s} \\ &= e^{-u/2r_s} e^{v/2r_s} \\ &= \mp UV. \end{aligned} \tag{2.15}$$

Substituting this result into Equation 2.14 yields an expression defining r as a function of U and V:

$$e^{r/r_s}\left(\frac{r}{r_s} - 1\right) = -UV. \tag{2.16}$$

We now have all the information required to rewrite the Schwarzschild metric in terms of the null Kruskal coordinates. We find that

$$\mathrm{d}s^2 = -\frac{32M^3}{r} e^{-r/2M} \mathrm{d}U\mathrm{d}V + r^2\mathrm{d}\Omega^2. \tag{2.17}$$

Unlike the metric in Equation 2.1, Equation 2.17 is nonsingular on the $r = r_s$ surface. By rewriting the Schwarzschild metric in null Kruskal coordinates U and V, we have succeeded in circumventing the singularity at $r = r_s$.

Figure 2.2 is a diagram depicting the Kruskal spacetime. Outgoing rays move along curves of constant U, and ingoing rays move along curves of constant V. Surfaces of constant r correspond to $UV = \text{const.}$, and as such there are two copies of each constant r surface in a Kruskal diagram. As an example, the $r = r_s$ surface corresponds to $UV = 0$ for which we could have either $U = 0$ or $V = 0$. Region I is the region of spacetime covered by the Schwarzschild coordinates. Use of the Kruskal coordinates facilitates the continuation of the Schwarzschild metric through the $r = 2M$ singularity into region II. We refer to the Kruskal coordinates as the 'maximal extension' of the Schwarzschild spacetime; the regions III and IV are not usually required and they exist only in the Kruskal representation.

2.3 Eddington-Finkelstein Coordinates

As mentioned above, regions III and IV in the Kruskal diagram are not generally required to describe the spacetime, and the Kruskal coordinates can be inconvenient when one is

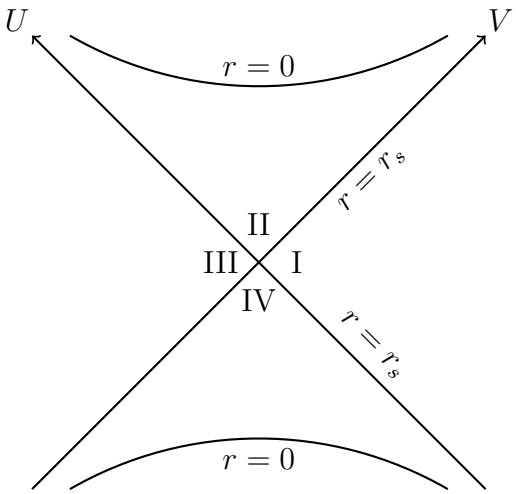

Figure 2.2: The Kruskal spacetime. Region I is described by the Schwarzschild coordinates, and the Kruskal coordinates allow continuation of the metric into region II. Regions III and IV exist only in the maximal extension of the Schwarzschild spacetime.

performing calculations. It therefore makes sense to define some simpler coordinates which are still nonsingular at $r = 2M$. Let u and v be defined as in Equations 2.3a and 2.3b. (v, r) and (u, r) are ingoing and outgoing Eddington-Finkelstein coordinates respectively. In ingoing Eddington-Finkelstein coordinates (v, r), the Schwarzschild metric (Equation 2.1) becomes

$$\mathrm{d}s^2 = -\left(1 - \frac{r_s}{r}\right)\mathrm{d}v^2 + 2\mathrm{d}v\mathrm{d}r + r^2\mathrm{d}\Omega^2. \tag{2.18}$$

The (v, r) coordinates represent regions I and II of the Kruskal diagram. In outgoing coordinates (u, r) the metric is

$$\mathrm{d}s^2 = -\left(1 - \frac{r_s}{r}\right)\mathrm{d}v^2 - 2\mathrm{d}u\mathrm{d}r + r^2\mathrm{d}\Omega^2, \tag{2.19}$$

and the (u, r) coordinates describe regions IV and I of Figure 2.2. Eddington-Finkelstein coordinates can be used to construct spacetime diagrams, but these diagrams will not have both ingoing and outgoing rays propagating at 45° as in the Kruskal diagram. Figure 2.3 is an Eddington-Finkelstein spacetime diagram. Ingoing rays move along paths defined by $\mathrm{d}v = 0$, i.e. oriented at 45°. The direction of outgoing rays is not constant, since $\frac{\mathrm{d}v}{\mathrm{d}r} = \frac{2}{1 - r_s/r}$.

2.4 Spacetime Diagram for the Schwarzschild Black Hole

Penrose diagrams are an extremely useful tool for illustrating the causal structure of a particular spacetime. Locally a Penrose diagram is conformally equivalent to the actual spacetime metric, meaning that angles are preserved. In order to represent the

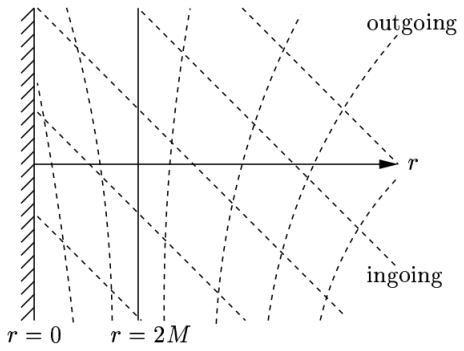

Figure 2.3: An Eddington-Finkelstein spacetime diagram, courtesy of [65].

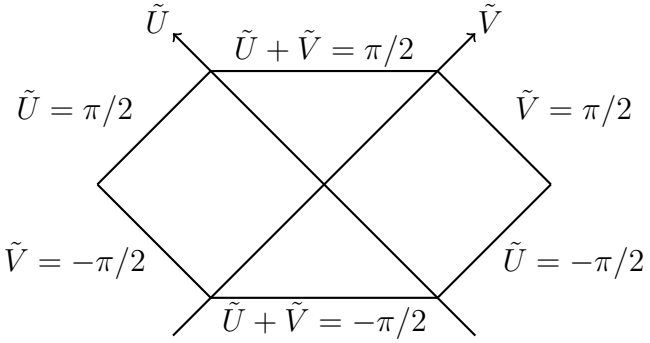

Figure 2.4: A spacetime diagram of the compactified coordinates defined by the transformations in Equations 2.20.

Schwarzschild spacetime using a Penrose diagram, we must first map the coordinates U and V defined in Section 2.2 into a finite domain. We do this by applying the transformations

$$\tilde{U} = \arctan U \tag{2.20a}$$

$$\text{and } \tilde{V} = \arctan V. \tag{2.20b}$$

These transformations are useful because they allow us to map the whole Schwarzschild spacetime described by the coordinates U and V, which have infinite range, into a finite domain in the $\tilde{U}$-$\tilde{V}$ plane. The disadvantage of this mapping is that it introduces new coordinate singularities at the boundaries of the spacetime. Figure 2.4 is a spacetime diagram of the compactified coordinates $\tilde{U}$ and $\tilde{V}$. In this diagram, the $r = r_s$ surfaces occur at $\tilde{U} = 0$ and $\tilde{V} = 0$. The singularities that were at $r = 0$ or $UV = 1$ are now at $\tilde{U} + \tilde{V} = \pm\frac{\pi}{2}$, and new singularities due to the transformation occur at $(\tilde{U}, \tilde{V}) = (\pm\frac{\pi}{2}, \pm\frac{\pi}{2})$.

Figure 2.5 is a Kruskal diagram of the Schwarzschild spacetime. The definitions of the diagram labels are as follows:

- $\mathscr{I}^+$ is 'future null infinity', and it defines the surfaces on which $\tilde{U} = \frac{\pi}{2}$ and $\tilde{V} = \frac{\pi}{2}$. It contains the future endpoints of all outgoing null geodesics.

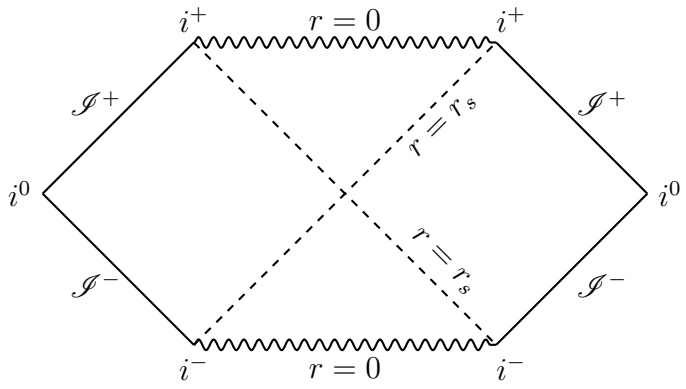

Figure 2.5: A Kruskal diagram of the Schwarzschild spacetime.

- $\mathscr{I}^-$ is 'past null infinity'. It defines the surfaces on which $\tilde{U} = -\frac{\pi}{2}$ and $\tilde{V} = -\frac{\pi}{2}$, and contains the past endpoints of all ingoing null geodesics.
- 'Spacelike infinity' i^0 represents the points at which $\mathscr{I}^+$ and $\mathscr{I}^-$ coincide. It contains the endpoints of all spacelike geodesics.
- 'Future timelike infinity' i^+ defines the points $(\tilde{U}, \tilde{V}) = (0, \frac{\pi}{2})$ and $(\tilde{U}, \tilde{V}) = (\frac{\pi}{2}, 0)$. It contains the future endpoints of all timelike geodesics that do not terminate at $r = 0$.
- 'Past timelike infinity' i^- defines the points $(\tilde{U}, \tilde{V}) = (0, -\frac{\pi}{2})$ and $(\tilde{U}, \tilde{V}) = (-\frac{\pi}{2}, 0)$. It contains the past endpoints of all timelike geodesics that do not begin at $r = 0$.

2.5 The Event Horizon & The Apparent Horizon

In a Kruskal diagram (see Figure 2.2), all light cones are tilted at 45°. This means that the timelike paths followed by the light cones are only able to move towards, and not away from the singularity at $r = 0$. Once an observer has crossed the surface $r = r_s$ that separates regions I and II of the Kruskal diagram, they are unable to return or to send signals out of the black hole. The crossing of this surface also means that an observer outside of the black hole would not be able to detect any signals coming from within. For this reason, we refer to the $r = r_s$ surface as the 'event horizon'. Region II, which is inside the event horizon of the black hole, is called the 'black hole region'. There is a second event horizon between regions IV and I, and we must therefore distinguish between these two event horizons. We call the event horizon between regions I and II the 'future horizon', and the 'past horizon' is the $r = r_s$ surface between regions IV and I. The region inside the past horizon of the black hole (region IV) is the 'white hole region'.

In order to define the 'apparent horizon' of a black hole, we must redefine the notions of 'outgoing' and 'ingoing' rays. We will now define outgoing rays as those which travel on curves of constant U, where r is not necessarily increasing. Similarly, ingoing rays are those which move on curves of constant V, and r is not necessarily decreasing. We can

show (see [65], for example) that the expansion of a congruence[1] of rays changes sign at $r = r_s$. We should also be able to see this from the fact that r increases along the geodesics that are outside $r = r_s$, but decreases along the geodesics that are inside. The expansion is positive for $U < 0$, which is in the past of $r = r_s$, and negative for $U > 0$ (in the future of $r = r_s$). We therefore refer to the $r = r_s$ surface in this context as the 'apparent horizon'. The concepts of 'event horizon' and 'apparent horizon' overlap; the differences between the two types of horizon only become apparent when the spacetime is no longer static (in a rotating black hole, for example).

2.6 The Killing Horizon

A Killing vector of the Schwarzschild spacetime is defined by

$$t^\alpha = \frac{\partial x^\alpha}{\partial t}. \tag{2.21}$$

t^α is timelike outside the black hole, null on the event horizon and spacelike inside the black hole, and it satisfies the equation

$$g_{\alpha\beta} t^\alpha t^\beta = 1 - \frac{r_s}{r}, \tag{2.22}$$

where $g_{\alpha\beta}$ is the spacetime metric. We refer to the $r = r_s$ surface as a 'Killing horizon', because the Killing vector field is null on this surface [16]. In a static black hole spacetime such as the one we are studying, the definitions of the event, apparent and Killing horizons all coincide.

2.7 Spacetime Diagram for the Black-to-White Hole Transition

In this thesis we explore the proposal that when a black hole has evaporated via Hawking radiation until its mass is on the scale of the Planck mass, it will undergo a quantum transition into a white hole: an object that is the time-reversal of the black hole. As stated in Section 1.1.3, this transition takes the form of quantum tunnelling. There are various ways in which we can represent the black-to-white hole transition using spacetime diagrams. We begin by looking at the Kruskal diagram for a Schwarzschild black hole (Figure 2.5) and considering a null shell falling into the black hole region and a second null shell that 'explodes' out of the white hole region. We then consider two different strategies for representing the physical spacetime, which we will refer to as

1. 'Untwisting' of the trajectories of the null shells.

2. Gluing of two Kruskal diagrams at the central Schwarzschild singularity.

[1] A congruence of curves is the set of integral curves defined by a nonvanishing vector field on the spacetime manifold.

1. 'Untwisting' of the Null Trajectories

Figure 2.6 is a Kruskal diagram of the Schwarzschild spacetime, with labels as defined in Section 2.4. The bold diagonal line with gradient -1 denotes a null shell that falls into the black hole region. $\mathcal{E}_0$ and $\mathcal{E}_1$ are the first moments in time that quantum effects dominate and the Einstein equations are violated, for the black and white hole regions respectively. A null shell 'explodes' out of the white hole region, as shown by the bold diagonal line with gradient 1. The corner $\mathcal{J}$ is the maximal extension in space of the region in which the Einstein equations are violated; we refer to it as the corner of the quantum gravity region. By 'untwisting' the trajectories of the null shells, we obtain the Penrose diagram in Figure 2.7. In this diagram, the bold diagonal lines again represent the infalling null shell (below) and the exploding null shell (above). The dashed lines are the black and white hole horizons. The lines joining $\mathcal{E}_1$ to $\mathcal{J}$ and $\mathcal{E}_0$ to $\mathcal{J}$ represent the boundaries of the quantum gravity region. In this study, we choose to define the boundary of the quantum gravity region by the surface on which the trace of the extrinsic curvature is zero ($K = 0$) and its time-reversal. We call these surfaces Σ_0 and Σ_1, and they meet at the corner $\mathcal{J} = \Sigma_0 \cap \Sigma_1$. We will see in Chapter 4 that the choice $K = 0$ causes the boundary term of the gravitational action to vanish and thus simplifies the calculation of the tunnelling amplitude for the black-to-white hole transition. The location of the corner $\mathcal{J}$ is as yet unclear. Intuitively we expect it to be near the horizon $r = r_s$, since the quantum transition occurs when the black hole horizon evolves into a white hole horizon. The corner $\mathcal{J}$ might be just inside the horizon, just outside or on the horizon itself. The location of the corner is critical in the calculation of the tunnelling probability, and we discuss this open question further in Chapter 7.

2. Gluing of Two Kruskal Diagrams

An alternative way to represent the black hole to white hole transition using a spacetime diagram is by gluing two Kruskal spacetimes at the central Schwarzschild singularity, as shown in Figure 2.8. As in Figure 2.6, the bold diagonal line with gradient -1 is the null shell falling into the black hole, and the corresponding line with gradient 1 is the null shell exploding out of the white hole. The shaded region is the portion of spacetime described by the metric of a black-to-white hole transition. Figure 2.9 shows the regions corresponding to the physical spacetime. The corner of the quantum gravity region $\mathcal{J}$ is located within the region denoted by the white diamond, which encloses the intersection of the black hole and white hole horizons. As mentioned above, it is as yet unclear whether $\mathcal{J}$ is inside, outside or on the horizon.

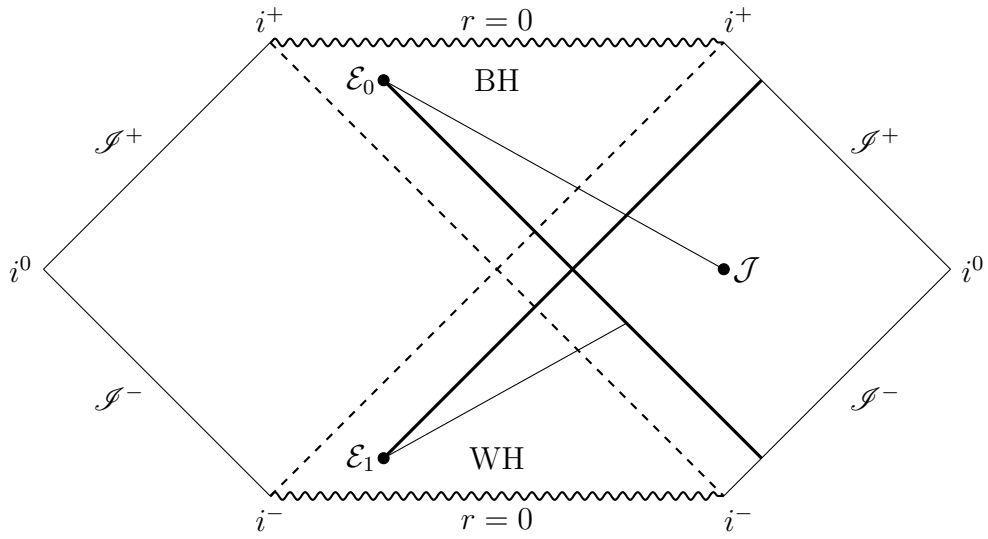

Figure 2.6: A Kruskal diagram of the Schwarzschild spacetime. A null shell falls into the black hole, and a second null shell 'explodes' out of the white hole. $\mathcal{E}_0$ and $\mathcal{E}_1$ are the first moments in time when Einstein's equations are violated for the black hole region and the white hole region respectively. $\mathcal{J}$ is the maximal extension in space of the region in which general relativity fails: we refer to $\mathcal{J}$ as the corner of the quantum gravity region.

2.8 Conclusion

In this chapter we reviewed the Schwarzschild black hole, and some of the different coordinate systems that we may use to describe it. We then considered two different ways in which to represent the physical spacetime of the tunnelling transition on a Penrose diagram. Since we would like to model the quantum tunnelling transition between a black hole and a white hole, it is important to revise the basics of the phenomenon of tunnelling. In the next chapter we do this with the aid of a simple example: tunnelling through a one-dimensional rectangular potential barrier. Feynman's path integral formulation and its implications for the probability of tunnelling through a classically forbidden region are also studied.

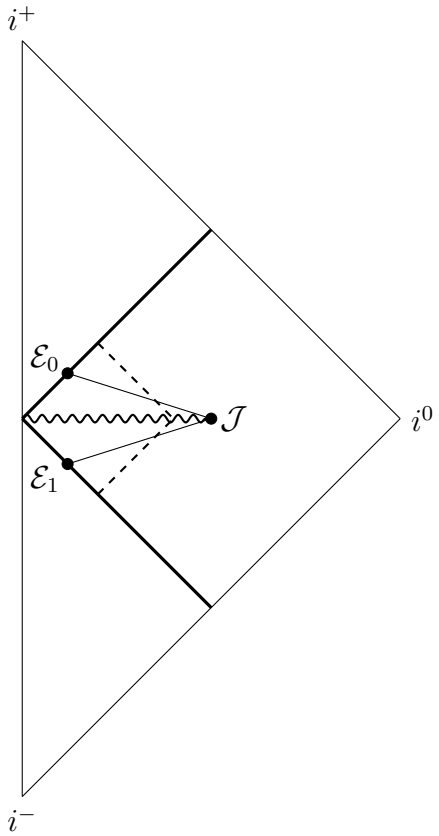

Figure 2.7: A Penrose diagram corresponding to the Kruskal diagram in Figure 2.6. By 'untwisting' the trajectories of the null shells, we obtain a diagram representing the physical black-to-white hole spacetime. The boundaries of the quantum gravity region are shown by the lines joining $\mathcal{E}_1$ to $\mathcal{J}$ and $\mathcal{E}_0$ to $\mathcal{J}$. In this thesis, we choose to define the boundary of the quantum gravity region by the surface on which the trace of the extrinsic curvature is zero ($K = 0$) and its time-reversal. The corner $\mathcal{J}$ may be located inside, outside or directly on the horizon.

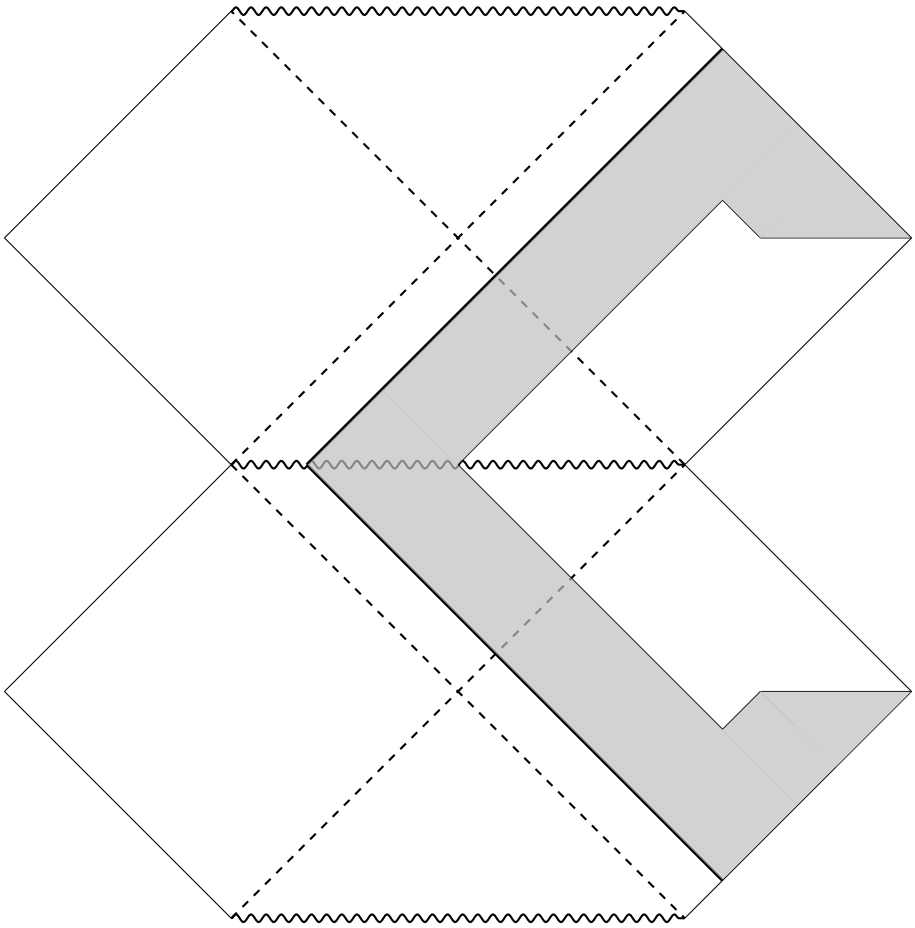

Figure 2.8: Two Kruskal spacetimes are glued at the central Schwarzschild singularity. The shaded region is the metric of a black-to-white hole transition outside a null shell falling into the black hole and a second null shell exploding out of the white hole.

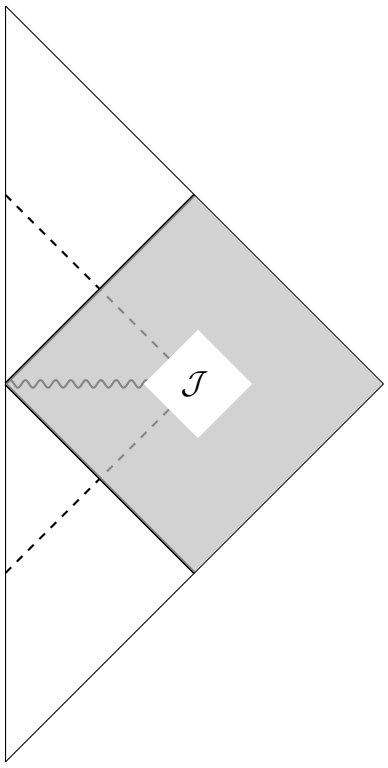

Figure 2.9: The Penrose diagram corresponding to the gluing of two Kruskal spacetimes in Figure 2.8. The bold diagonal lines are the null shell collapsing into the black hole (below) and the null shell exploding out of the white hole (above). The corner of the quantum gravity region $\mathcal{J}$ is located within the region denoted by the white diamond, which encloses the intersection of the black hole and white hole horizons. It is as yet unclear whether $\mathcal{J}$ is inside, outside or on the horizon.

Chapter 3

Quantum Tunnelling

Since the black-to-white hole transition takes the form of quantum tunnelling, it is important to review the basics of tunnelling theory. In this chapter, we study quantum tunnelling using two different approaches: first the solution of the time-independent Schrödinger equation, and then the path integral formalism. In both cases we use the simple example of one-dimensional tunnelling through a potential barrier. Finally we discuss how the path integral formalism is used to obtain the coefficient of transmission through the potential barrier. In this chapter we will leave $\hbar$ explicit in the equations, as is convention in quantum mechanics calculations.

3.1 Historical Remarks

The phenomenon of quantum tunnelling originates from Henri Becquerel's discovery of natural radioactivity in 1896 [69]. Nuclear radioactivity is governed by the well-known exponential decay law,

$$\begin{aligned} \frac{\mathrm{d}N(t)}{\mathrm{d}t} &= -\Gamma N(t) \\ &\Rightarrow N(t) = N_0 \exp(-\Gamma t) \end{aligned} \tag{3.1}$$

where N_0 is the initial number of nuclei (at time $t = 0$), $N(t)$ is the number of nuclei at time $t > 0$ and Γ is the probability of decay per unit time. The exponential decay law may also be written in terms of $P(t)$, the probability that an individual nucleus has not decayed at time t:

$$P(t) = \frac{N(t)}{N_0} = e^{-\Gamma t}. \tag{3.2}$$

Quantum tunnelling in its most familiar form first emerged via George Gamow's description of α-decay [37–39]. The emission of an α-particle by a nucleus is a classically forbidden process. Gamow modelled the α-particle as being trapped inside a potential well by the nucleus, and used the laws of quantum mechanics to show that there is a finite probability

that the α-particle can escape this potential well via quantum tunnelling and thus be emitted from the nucleus. Upon solving the Schrödinger equation for this potential, he found that the only solutions were those with complex energies. By interpreting the complex part of the energy as $\frac{\Gamma}{2}$ [70], Gamow recovered the Geiger-Nuttall law which relates the half-life of the decay to the energy of the α-particle. Gamow also realised that the phenomenon of quantum tunnelling is relevant in nuclear reactions; the famous 'Gamow factor' is a measure of the probability of two nuclei tunnelling through the Coulomb barrier in order to undergo a reaction such as nuclear fusion. Following this work by Gamow, Max Born is credited with the realization that amongst many other physical phenomena, quantum tunnelling may be used to describe the emission of electrons from the surface of a cold metal ('cold emission').

3.2 Basics of Quantum Tunnelling

3.2.1 Heisenberg's Uncertainty Principle

Tunnelling has no classical counterpart: it is a purely quantum effect. The total energy of the tunnelling particle is given by

$$E = \frac{1}{2m}p^2 + V(x) \tag{3.3}$$

where m is the mass of the particle, p is its momentum and $\frac{1}{2m}p^2$ is its kinetic energy. $V(x)$ is the height of the potential barrier. From Equation 3.3, it seems that if the energy of the particle is less than the height of the potential barrier, its kinetic energy will be negative and its momentum will therefore be imaginary. However, this is incorrect since so far we have not considered the effect of Heisenberg's Uncertainty Principle. The Uncertainty Principle tells us that it is impossible to know both the position and momentum of the particle with certainty at any one instant in time; if the particle is at the point x with $E < V(x)$, its momentum p is uncertain by an amount $\sqrt{\overline{\Delta p^2}}$. It can be shown (see [71], for example) that the kinetic energy of the particle must be greater than the difference between the height of the barrier and the total energy of the particle.

3.2.2 Tunnelling Through a Rectangular Potential Barrier

In order to illustrate the phenomenon of quantum tunnelling, we will now look at a simple example in one dimension: the rectangular potential barrier. The potential barrier is defined by

$$V(x) = \begin{cases} 0 & x < 0 \\ V_0 & 0 \leq x \leq L \\ 0 & x > L, \end{cases} \tag{3.4}$$

as illustrated in Figure 3.1. We will refer to the regions on the left hand side, inside

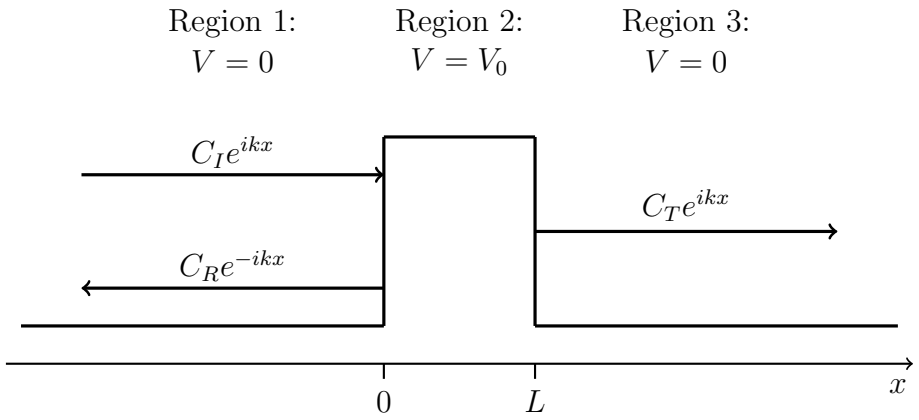

Figure 3.1: The rectangular potential barrier defined in Equation 3.4.

the potential barrier and on the right hand side as 1, 2 and 3 respectively. Classically, a particle with energy $E < V_0$ would be reflected off the potential barrier and travel in the opposite direction along the x-axis, whilst a particle with $E > V_0$ would be transmitted through the barrier. Quantum mechanics says that there is a small but finite probability that a particle with $E < V_0$ will tunnel through the potential barrier and emerge on the other side.

The one-dimensional time-independent Schrödinger equation is

$$\left[-\frac{\hbar^2}{2m}\frac{\mathrm{d}^2}{\mathrm{d}x^2} + V(x) \right] u(x) = Eu(x) \tag{3.5}$$

where the particle has momentum $\hbar k$ and kinetic energy $\frac{\hbar^2 k^2}{2m}$, and k is the wavenumber. In Region 1, the solution to this equation is

$$u(x) = C_I e^{ikx} + C_R e^{-ikx}, \tag{3.6}$$

where $|C_I|^2$ and $|C_R|^2$ are the intensities of the wave incoming from the left and the wave reflected back off the potential barrier respectively. In Region 2, the solution to Equation 3.5 is dependent on whether the energy of the particle is greater or less than the height of the potential barrier. For $E > V_0$, we may write the general solution as

$$u(x) = Be^{ik_U x} + B'e^{-ik_U x} \tag{3.7}$$

where $k_U = \frac{\sqrt{2m(E-V_0)}}{\hbar}$ and B and B' are constants. If $E < V_0$, the general solution is

$$u(x) = De^{-\alpha x} + D'e^{\alpha x} \tag{3.8}$$

where $\alpha = \frac{\sqrt{2m(V_0-E)}}{\hbar}$ and D and D' are constants. The solution for $E < V_0$ is classically forbidden. In Region 3, the solution to the time-independent Schrödinger equation is

$$u(x) = C_T e^{ikx} \tag{3.9}$$

where $k = \frac{\sqrt{2mE}}{\hbar}$ and $|C_T|^2$ is the intensity of the wave after passing through the potential barrier. Using the condition that both $u(x)$ and $\frac{\mathrm{d}u(x)}{\mathrm{d}x}$ must be continuous at $x = 0$ and $x = L$, we find that

$$\text{at } x = 0: \qquad C_I + C_R = D + D' \tag{3.10}$$

$$ik(C_I - C_R) = -\alpha(D - D') \tag{3.11}$$

$$\text{at } x = L: \qquad De^{-\alpha L} + D'e^{\alpha L} = C_T e^{ikL} \tag{3.12}$$

$$-\alpha(De^{-\alpha L} - D'e^{\alpha L}) = ikC_T e^{ikL}. \tag{3.13}$$

Since the probability that the particle is at position x is proportional to $|u(x)|^2$, the probability that it will be reflected at $x = 0$ is given by

$$R = \frac{|C_R|^2}{|C_I|^2}, \tag{3.14}$$

while the probability that the particle will be transmitted through the barrier and into Region 3 is

$$T = \frac{|C_T|^2}{|C_I|^2}. \tag{3.15}$$

Making the approximation that the potential barrier is wide such that $\alpha L \gg 1$ and solving Equations 3.10-3.13 simultaneously, we arrive at an expression for the probability that the particle will be transmitted through the barrier:

$$T = \frac{|C_T|^2}{|C_I|^2} = \frac{16\alpha^2 k^2 e^{-2\alpha L}}{(k^2 + \alpha^2)^2}. \tag{3.16}$$

Substituting in $k = \frac{\sqrt{2mE}}{\hbar}$ and $\alpha = \frac{\sqrt{2m(V_0 - E)}}{\hbar}$, we find that

$$T = 16\left(\frac{E(V_0 - E)}{V_0^2}\right)e^{-2\sqrt{2m(V_0 - E)}L/\hbar} \tag{3.17}$$

which is the probability that when $E < V_0$, the particle will travel through the classically forbidden region. This probability is an exponentially decaying function of

- The square root of the width of the potential barrier, $\sqrt{L}$.
- The square root of the particle's mass, $\sqrt{m}$.
- The square root of the difference between the barrier height and the energy of the particle, $\sqrt{(V_0 - E)}$.

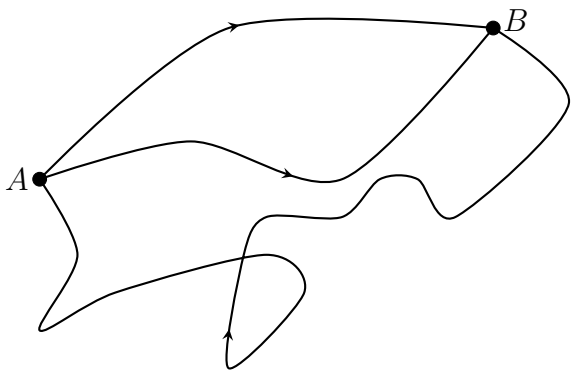

Figure 3.2: Three of the infinite number of trajectories that contribute to the quantum amplitude of a particle travelling from point A to point B.

3.3 The Path Integral Approach to Quantum Tunnelling

An alternative way to model the quantum tunnelling process is using the path integral formulation of quantum mechanics [31]. The path integral formulation is a generalisation of the principle of least action in classical mechanics. Consider a particle moving from an initial spacetime point A to a final point B. Classically, the path of the particle is described by a single unique trajectory. The path integral approach replaces the single trajectory with a sum over the infinite number of paths that are allowed by quantum mechanics; this sum is referred to as the 'quantum amplitude' (see Figure 3.2). The concept of the path integral was first introduced by Norbert Wiener as a method of solving problems related to Brownian motion [20, 87]. The idea was further developed by Paul Dirac in his 1933 paper on the principle of least action and the quantum analogue of classical Lagrangian theory [29]. However, the colossal success of the path integral formulation is attributed to Richard Feynman, who was the first to show that the Schrödinger equation and the canonical commutation relations of quantum mechanics can be recovered using path integrals [32,33]. Feynman was also able to show that in the classical limit $\hbar \to 0$, the classical path arises naturally. There are several different ways to derive the path integral formulation, including the time-slicing derivation [21]. In this section we will not detail the full derivation; instead, we will first introduce the key concepts and give a more qualitative description of the path integral approach. We will then give a simple example, where the path integral formulation is used to describe the quantum tunnelling of a particle through a one-dimensional potential barrier.

In order to prove the success of the path integral formulation, it was essential to show that we can recover the results of quantum mechanics from it. For this purpose, Feynman postulated that:

1. The probability that a particle initially at point A will be at point B at a given time is the squared modulus of a complex number called the 'probability amplitude'.

2. The probability amplitude is obtained by adding together the contributions of all possible paths allowed by quantum mechanics.

3. The contribution of an individual path is proportional to $e^{iS/\hbar}$, where S is the action given by the time integral of the Lagrangian along the path.

The sum over paths becomes an integral because the number of possible paths for any given process is infinite. To find the probability amplitude for a given process, we integrate the contribution of a path (postulate 3) over the space of all possible paths in between the initial and final state, including the paths that are forbidden by classical mechanics. Each path contributes equally in magnitude. However, the 'phase' of their contribution varies from path to path. The phase is given by the classical action: the time integral of the Lagrangian of the path [3]. This quantity will be different for each path. The varying phase is important, because it allows individual paths to interfere with each other.

3.3.1 Path Integral for the One-Dimensional Potential Barrier

As a simple example, we consider a particle which quantum tunnels through a one-dimensional potential barrier. We must first introduce the 'Feynman propagator' $D_F(x_f, x_i; T, 0)$, defined by the transition amplitude

$$D_F(x_f, x_i; T, 0) = \langle x_f | \hat{U}(T, 0) | x_i \rangle \tag{3.18}$$

where $\hat{U}(T, 0)$ is the unitary time-evolution operator for the system,

$$\hat{U}(T, 0) = \exp\left[\frac{iH(T-0)}{\hbar}\right] \tag{3.19}$$

and H is the Hamiltonian. The square root of the absolute value of D_F is a measure of the probability that a particle which is initially at position $x = x_i$ will be at $x = x_f$ at time T [72]. The propagator is dependent on the integral over all possible paths of the particle, i.e.

$$D_F \sim \int [\mathcal{D}(x)] \exp\left[\frac{i}{\hbar} S(x)\right] \tag{3.20}$$

where $S(x)$ is the action corresponding to each path. It is clear from Equation 3.20 that the probability amplitude A of a quantum transition is proportional to $e^{iS/\hbar}$, i.e. $A \sim e^{iS/\hbar}$. It can be useful to replace $D_F(x_f, x_i; T, 0)$ with its energy Fourier transform,

$$D_F(x_f, x_i; E) = \int_0^\infty \exp\left(\frac{iET}{\hbar}\right) D_F(x_f, x_i; T, 0)\, dT. \tag{3.21}$$

In the classical limit, i.e. $\hbar \to 0$, we can use the stationary phase method to find an approximate expression for the Feynman propagator. For details, see [52]. We find that

$$D_F(x_f, x_i; T, 0) \approx f(x_f, x_i) \exp(iS[x_{cl}]/\hbar) \tag{3.22}$$

where

$$f(x_f, x_i) = \frac{1}{\left[2i\pi k(x_f) k(x_i) \int_{x_i}^{x_f} \frac{dx}{(k(x))^3}\right]^{1/2}} \tag{3.23}$$

and $S[x_{cl}]$ is the classical action for the path from $(x_i, 0)$ to (x_f, T). $S[x_{cl}]$ is given by

$$S[x_{cl}] = \int_{x_i}^{x_f} \sqrt{2m[E_{cl} - V(x)]}\, dx - E_{cl}T' \tag{3.24}$$

where E_{cl} is the classical energy of the path, related to T' by

$$T' = \int_{x_i}^{x_f} \sqrt{\frac{m}{2[E_{cl} - V(x)]}}\, dx. \tag{3.25}$$

Applying the stationary phase method to the energy Fourier transform of D_F (Equation 3.21) yields

$$D_F(x_f, x_i; E) \approx \frac{m}{\sqrt{k(x_f)k(x_i)}} \exp\left[i \int_{x_i}^{x_f} k_{cl}(x)dx\right] \tag{3.26}$$

where the wavenumber k satisfies

$$k^2 = \frac{2mE}{\hbar^2}. \tag{3.27}$$

The approximation in Equation 3.26 is valid only for paths which are classically allowed; it does not hold for the cases where quantum tunnelling occurs. However, we can generalise the propagator to include tunnelling trajectories. Let all paths, classical and non-classical, be denoted by x_n. We can then write the propagator as

$$D_F(x_f, x_i; E) = \frac{m}{\sqrt{k(x_f)k(x_i)}} \sum_n K_n \tag{3.28}$$

where the coefficients K_n are determined by two rules:

1. The exponential factor in the propagator is dependent on whether the path is classically allowed or classically forbidden. In the classically allowed region, we use the factor

$$\exp\left[i \int_{x_1}^{x_2} k(x)dx\right] \tag{3.29}$$

where $k(x) = \sqrt{k^2 - V(x)}$. In the classically forbidden region, we instead use the factor

$$\exp\left[-\int_{x_1}^{x_2} q(x)dx\right] \tag{3.30}$$

where $q(x) = \sqrt{V(x) - k^2}$.

2. If the particle is reflected from a turning point where classical motion is allowed, we use a factor $(-i)$. If the reflection is from a region where classical motion is forbidden, we use a factor $(-i/2)$.

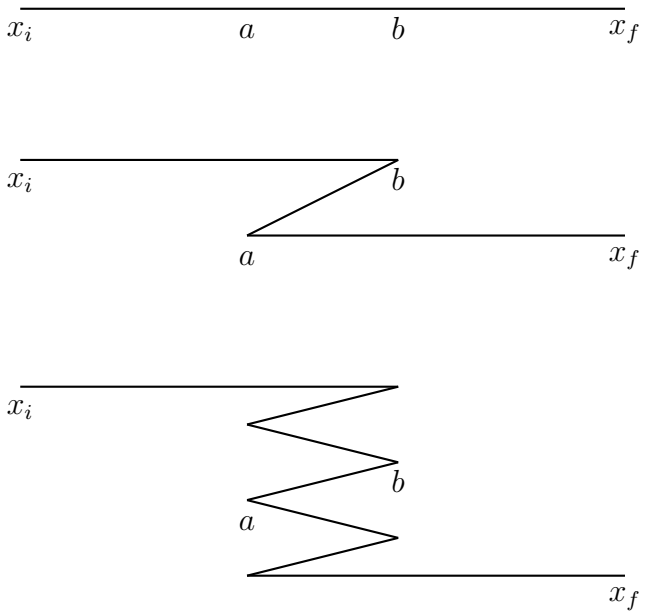

Figure 3.3: Some of the possible paths taken by the particle from x_i to x_f. $a(E)$ and $b(E)$ are turning points of the potential barrier. The particle may undergo reflections inside the barrier, as shown in the lower two diagrams.

Constructing the Propagator in the Classically Forbidden Region

Consider a one-dimensional potential barrier with turning points at $a(E)$ and $b(E)$, where $b(E) > a(E)$. The particle is initially at position $x = x_i$ to the left of $a(E)$, and its final position is $x = x_f$ (to the right of $b(E)$). It may travel straight through the barrier or be reflected a number of times inside the barrier, as can be seen in Figure 3.3. In a similar fashion to Section 3.2.2, we can study the motion of the particle in three distinct regions:

- **Region 1:** from the initial position $x = x_i$ to $x = a(E)$.
- **Region 2:** propagation through the classically forbidden region from $a(E)$ to $b(E)$.
- **Region 3:** from $x = b(E)$ to the final position at $x = x_f$.

The Feynman propagator D_F can then be written as

$$\begin{aligned} D_F(x_f, x_i; E) = \frac{m}{\sqrt{k(x_f)k(x_i)}} \exp\left[i\int_{x_i}^{a} k(x)dx\right] \\ \times \left\{Z + \left(\frac{i}{2}\right)^2 Z^3 + \left(\frac{i}{2}\right)^4 Z^5 + \dots\right\} \\ \times \exp\left[i\int_{b}^{x_f} k(x)dx\right] \end{aligned} \tag{3.31}$$

where

$$Z = \exp\left[-\int_a^b q(x)dx\right] \tag{3.32}$$

is the 'penetration factor' that arises in the WKB approximation. The expression in curly brackets in Equation 3.31 is an infinite geometric series, and we can therefore simplify it using the well-known formula for the sum of an infinite geometric series:

$$\sum_{k=0}^{\infty} ar^k = \frac{a}{1-r} \tag{3.33}$$

where a is the first term in the series and r is the common ratio between terms. Equation 3.33 is valid only for convergent series, i.e. series with $|r| < 1$. For the series in Equation 3.31 we have $a = Z$ and $r = (\frac{i}{2})^2 Z^2$, and so

$$\sum_{k=0}^{\infty} ar^k = \frac{Z}{1-\left(\frac{i}{2}\right)^2 Z^2} = \frac{Z}{1+\frac{1}{4}Z^2}. \tag{3.34}$$

Substituting this into Equation 3.31 we find that

$$\begin{aligned} D_F(x_f, x_i; E) = {} & \frac{m}{\sqrt{k(x_f)k(x_i)}} \exp\left[i\int_{x_i}^{a} k(x)dx\right] \\ & \times \left(\frac{Z}{1+\frac{1}{4}Z^2}\right) \exp\left[i\int_{b}^{x_f} k(x)dx\right]. \end{aligned} \tag{3.35}$$

The first exponential in the above expression for the propagator corresponds to motion from the particle's initial position at x_i to the barrier, and the Z term represents propagation in the classically forbidden region (or 'under the barrier'). The last exponential describes motion from the barrier to the final position at x_f. We can therefore write the coefficient of transmission through the barrier as

$$|T(E)|^2 = \left|\frac{Z}{1+\frac{1}{4}Z^2}\right|^2. \tag{3.36}$$

3.4 Conclusion

In this chapter we reviewed the phenomenon of quantum tunnelling. We began with some historical remarks and then described the basics of tunnelling with the aid of a simple example: the one-dimensional rectangular potential barrier. By solving the time-independent Schrödinger equation in three separate regions (the left hand side of the potential barrier, inside the barrier and on the right hand side) and implementing continuity conditions on the solution and its derivative, we derived an expression for the probability that a particle will quantum tunnel through the classically forbidden region. We then considered how quantum tunnelling can alternatively be described using Feynman's path integral approach. We constructed the propagator for the one-dimensional potential barrier in

the classically forbidden region, and derived an equation for the coefficient of transmission through the barrier. In the next chapter we specify to the Schwarzschild spacetime, and deduce the total gravitational action for the region in which general relativity is violated (the quantum gravity region).

Chapter 4

Gravitational Action & The Corner Term

In Chapter 3, we discussed the result from Feynman's path integral formalism that the probability amplitude A of a quantum transition is proportional to the exponential of the complex number i multiplied by the action S:

$$A \sim e^{iS} \tag{4.1}$$

where for simplicity we have employed natural units $\hbar = 1$. Since we want to describe the transition between a black hole and a white hole, in this case the action S will be the gravitational action of our spacetime. Note that in order for quantum tunnelling to occur, we expect the gravitational action to have a finite imaginary part. We begin by specifying a four-dimensional spacetime manifold $\mathcal{M}$ with Lorentzian metric $g_{\mu\nu}$ where μ and ν are spacetime indices, $\mu, \nu = 0, 1, 2, 3$. The metric signature is $(-, +, +, +)$. We define the quantum gravity region as enclosed by intersecting hypersurfaces on which the trace of the extrinsic curvature is equal to zero, as shown in Figure 4.1. The hypersurfaces Σ_0 and Σ_1 meet at the corner $\mathcal{J} = \Sigma_0 \cap \Sigma_1$. The boundary of the quantum gravity region is the union of the hypersurfaces, i.e. $\Sigma_0 \cup \Sigma_1$. The gravitational action of our spacetime is composed of three terms corresponding to the bulk, the boundary of the quantum gravity region and the action at the corner $\mathcal{J}$ [49, 50]:

$$S = S_{EH} + S_B + S_C. \tag{4.2}$$

S_{EH} is the Einstein-Hilbert action

$$S_{EH} = \int R\sqrt{-g}\, d^4x, \tag{4.3}$$

where $g = \det(g_{\mu\nu})$ and R is the Ricci scalar. S_B is the boundary action and S_C is the action at the corner. Following Jubb et al. [54], we may express the Einstein-Hilbert action in an alternative way using Cartan's tetrad formalism. We introduce a tetrad 1-form e^I and a Lorentz connection A^{IJ}. The field strength of A is given by [54]

$$F^{IJ} = dA^{IJ} + A^I_K \wedge A^{KJ} = 2\mathcal{D}A^{IJ} \tag{4.4}$$

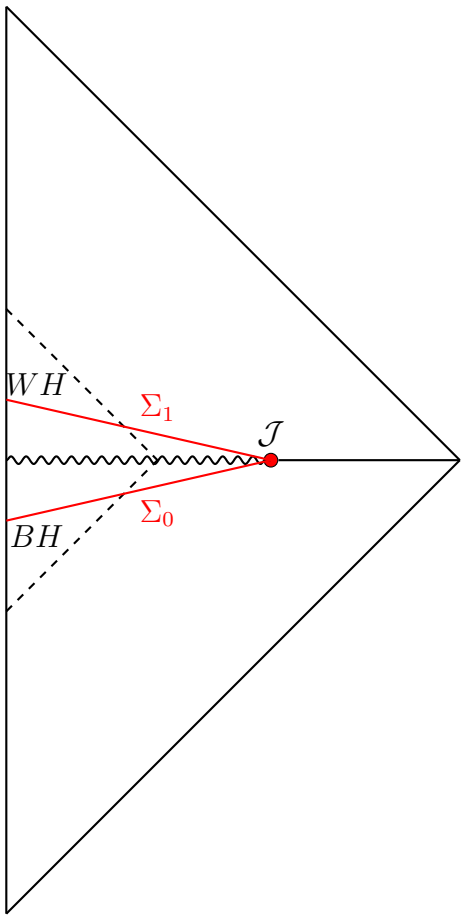

Figure 4.1: A Penrose diagram depicting the black-to-white hole transition. The 'quantum gravity region' is enclosed by the hypersurfaces Σ_0 and Σ_1, on which the trace of the extrinsic curvature is equal to zero. The hypersurfaces meet at the corner $\mathcal{J} = \Sigma_0 \cap \Sigma_1$. The infalling and exploding null shells discussed in Section 2.7 are not shown in this diagram.

where the wedge product is with respect to the spacetime indices. In terms of these quantities, the Einstein-Hilbert action takes the form

$$S_{EH} = \frac{1}{4}\int_{\mathcal{M}} d^4x \epsilon_{IJKM} e^I \wedge e^J \wedge F^{KM}(A) \tag{4.5}$$

where $I, J, K, M = 0, 1, 2, 3$ are internal indices. The variation of S_{EH} results in a bulk term and a boundary term. Taking the variation of Equation 4.5 gives

$$\begin{aligned}
\delta S_{EH} &= \frac{1}{4}\left(\int_{\mathcal{M}} \epsilon_{IJKM} \delta e^I \wedge e^J \wedge F^{KM} + \int_{\mathcal{M}} \epsilon_{IJKM} e^I \wedge \delta e^J \wedge F^{KM} + \int_{\mathcal{M}} \epsilon_{IJKM} e^I \wedge e^J \wedge \delta F^{KM} \right) \\
&= \frac{1}{4}\left(2\int_{\mathcal{M}} \epsilon_{IJKM} \delta e^I \wedge e^J \wedge F^{KM} + \int_{\mathcal{M}} \epsilon_{IJKM} e^I \wedge e^J \wedge \delta F^{KM} \right) \\
&= \frac{1}{4}\left(2\int_{\mathcal{M}} \epsilon_{IJKM} \delta e^I \wedge e^J \wedge F^{KM} + \int_{\mathcal{M}} \epsilon_{IJKM} e^I \wedge e^J \wedge \delta 2\mathcal{D} A^{KM} \right) \\
&= \frac{1}{4}\left(2\int_{\mathcal{M}} \epsilon_{IJKM} \delta e^I \wedge e^J \wedge F^{KM} + 2\int_{\mathcal{M}} \epsilon_{IJKM} e^I \wedge e^J \wedge \mathcal{D}\delta A^{KM} \right)
\end{aligned} \tag{4.6}$$

where in the second line we used the fact that the first two integrals are equal, and in the third line we used Equation 4.4 to write the field strength F^{KM} in terms of the connection A^{KM}. The first term in the above equation (the bulk term) yields Einstein's vacuum equations in the form

$$\epsilon_{IJKM} e^J \wedge F^{KM} = 0. \tag{4.7}$$

The boundary term is expressed as the variation of the boundary action $-S_B$, which gives us a counterterm to be added to the total gravitational action. We require that the pullback[1] of the metric to the boundary $\Sigma_0 \cup \Sigma_1$ has zero variation. This permits us to move the D in the second term to the front of the integral:

$$-\delta S_B = \frac{1}{2}\int_{\mathcal{M}} D(\epsilon_{IJKM} e^I \wedge e^J \wedge \delta A^{KM}). \tag{4.8}$$

We can then use Stokes' theorem to rewrite this as an integral over $\Sigma_0 \cup \Sigma_1$:

$$\begin{aligned}
-\delta S_B &= \frac{1}{2}\int_{\mathcal{M}} D(\epsilon_{IJKM} e^I \wedge e^J \wedge \delta A^{KM}) \\
&= +\frac{1}{2}\int_{\Sigma_0 \cup \Sigma_1} \epsilon_{IJKM} e^I \wedge e^J \wedge \delta A^{KM}.
\end{aligned} \tag{4.9}$$

Since δ acts only on the connection A^{KM}, we can take it outside of the integral:

$$-\delta S_B = \frac{1}{2}\delta \int_{\Sigma_0 \cup \Sigma_1} \epsilon_{IJKM} e^I \wedge e^J \wedge A^{KM}, \tag{4.10}$$

[1]Suppose that $\phi : M \to N$ is a smooth map between smooth manifolds M and N; then there is an associated linear map from the space of 1-forms on N to the space of 1-forms on M. Any covariant tensor field (any differential form) may be pulled back to M using ϕ.

and then

$$-S_B = \frac{1}{2}\int_{\Sigma_0\cup\Sigma_1} \epsilon_{IJKM} e^I \wedge e^J \wedge A^{KM} \tag{4.11}$$

or

$$S_B = -\frac{1}{2}\int_{\Sigma_0\cup\Sigma_1} \epsilon_{IJKM} e^I \wedge e^J \wedge A^{KM}. \tag{4.12}$$

So far, we have not specified whether the boundary $\Sigma_0 \cup \Sigma_1$ is spacelike, timelike or null. We will see in Chapter 5 that the boundary of our spacetime is necessarily spacelike. We now choose 'adapted tetrads' so that one of the 1-form fields e^I is normal to $\Sigma_0 \cup \Sigma_1$. By decomposing the metric $g_{\mu\nu}$ into components along Σ and transverse to it, where Σ is a single component of the boundary, we find that S_B reduces to the expected Gibbons-Hawking-York (GHY) term:

$$S_B = \int \sqrt{h} K d^3x \tag{4.13}$$

where the xs are coordinates on the boundary. h is the determinant of the induced metric h_{ab} on Σ, and $K = h^{ab}\nabla_a n_b$ is the trace of the extrinsic curvature where n_b is the normal covector to $\Sigma_0 \cup \Sigma_1$. For details of this calculation, see [54]. Equation 4.12 is not invariant under $O(1,3)$ transformations, because A transforms inhomogeneously by

$$A \to \Lambda^{-1} A \Lambda + \Lambda^{-1} d\Lambda, \tag{4.14}$$

and therefore

$$S_B \to S_B + \frac{1}{2}\int_{\Sigma_0\cup\Sigma_1} \epsilon_{IJKM} e^I \wedge e^J \wedge \mathbf{g}^{KM} \tag{4.15}$$

where $\mathbf{g} = \Lambda^{-1} d\Lambda$ is in the Lie algebra of $O(1,3)$. We can use this gauge invariance to find the final part of the full gravitational action: the corner term S_C. The adapted frames will not generally agree at the join of two boundary components; we need some method for passing from one frame to the other. The method we use is as follows:

1. Make a gauge transformation in the little group[2] H to make sure that two of the frame fields from each boundary component are tangent to the join, and agree with each other at the join.

2. Use discrete elements in $O(1,3)$ to ensure that the frames are related by an element in the identity component of $O(1,3)$.

3. The two frames are related by a Lorentz transformation in the two-dimensional plane of normals.

4. The corner terms are given by the change in Equation 4.12 under this $O(1,3)$ gauge transformation.

[2]The little group H preserves the normal. It is defined by $H = O(1,2)$ for spacelike normals.

We first let the spacelike hypersurfaces Σ_i and Σ_j meet along a join $\mathcal{J}_{ij}$. These hypersurfaces enclose the region of spacetime we are interested in studying. $e^I_{(i)}$ and $e^I_{(j)}$ are the adapted frames of Σ_i and Σ_j respectively. Through gauge transformations in the little group H, we can arrange that $e^2_{(i)} = e^2_{(j)}$ and $e^3_{(i)} = e^3_{(j)}$, and that both of these are orthogonal to the timelike plane of normals. This means that the frames $e_{(i)}$ and $e_{(j)}$ are related by a Lorentz boost in the timelike plane of normals:

$$e^I_{(i)} = \Lambda_{(ij)}{}^I_J e^J_{(j)}. \tag{4.16}$$

We define the discontinuous gauge transformation $\lambda \in O(1,1)$ to be the identity on Σ_i and $\Lambda_{(ij)}$ on Σ_j:

$$\lambda_{ij} = \exp\left[\eta K \Theta^{(H)}_{ij}\right] \tag{4.17}$$

where $\Theta^{(H)}_{ij}$ is the Heaviside function, equal to 0 on Σ_i and 1 on Σ_j. η is the boost angle between the normals to Σ_i and Σ_j, and K is the boost generator. $\mathbf{g}^{KM} = (\Lambda^{-1}_{(ij)} d\Lambda_{(ij)})^{KM} = \eta K^{KM} d\Theta^{(H)}_{ij}$ is proportional to a delta function that is peaked on the join and vanishes on Σ_i and Σ_j. Applying the gauge transformation to the boundary term (Equation 4.15) yields the join term

$$\frac{1}{2}\int_{\mathcal{J}_{ij}} \eta \epsilon_{IJKM} e^I \wedge e^J K^{KM}. \tag{4.18}$$

The only non-vanishing terms in the above expression are $K^{01} = -K^{10}$, so we find that the corner term is defined by

$$S_C \equiv S_{\mathcal{J}_{ij}} = \int_{\mathcal{J}_{ij}} e^2 \wedge e^3 \eta = \int_{\mathcal{J}_{ij}} dA\eta \tag{4.19}$$

where dA is the area element of the join. We have thus shown that the corner term of the gravitational action is dependent only on η, the boost angle between the normals to the hypersurfaces Σ_i and Σ_j. If the two normal vectors to the hypersurfaces are both timelike, the boost angle is defined by

$$\cosh \eta = -n_i \cdot n_j \tag{4.20}$$

where n_i and n_j are the normals to Σ_i and Σ_j respectively [54].

As previously mentioned, we choose to define the quantum gravity region as enclosed by the hypersurface on which the trace of the extrinsic curvature is zero ($K = 0$) and its time reversal. Solving Einstein's vacuum equations in the bulk with no cosmological constant results in a vanishing Ricci scalar, $R = 0$. This means that the Einstein-Hilbert action defined in Equation 4.3 will be equal to zero, and it will not yield a contribution to the full gravitational action S (Equation 4.2). We showed that the boundary term S_B (Equation 4.13) is dependent on the extrinsic curvature K. As we are only considering the surfaces on which $K = 0$, the boundary action of our spacetime will also vanish. We conclude that the only contribution to S comes from the action at the corner S_C. The Schwarzschild geometry is spherically symmetric, which means that the corner term reduces to

$$S_C = \int_{\mathcal{J}_{ij}} dA\eta = 4\pi r^2 \eta \tag{4.21}$$

where r is the radius of the corner. The full gravitational action, Equation 4.2, is then simply

$$S = S_C = 4\pi r^2 \eta. \tag{4.22}$$

We note that if we were instead dealing with timelike hypersurfaces, we would find that the corner term of the action is equal to Equation 4.19 for the spacelike case [54]. The null case, however, is different: when the hypersurfaces are null, there is no longer a rotation in the plane of normals. This means that the boost angle η must be equal to zero, and the corner term (Equation 4.19) will therefore vanish.

4.1 Conclusion

In this chapter we deduced the gravitational action for the spacetime we are interested in studying: a Schwarzschild black hole that quantum tunnels into a white hole. The total gravitational action is composed of three terms corresponding to the bulk of the quantum gravity region, the boundary and the corner $\mathcal{J}$. The bulk term is given by the standard Einstein-Hilbert action $S_{EH} = \int R\sqrt{-g}\ d^4x$. Solving Einstein's vacuum equations in the bulk with zero cosmological constant results in $R = 0$, and the bulk term of the gravitational action therefore vanishes. We showed that the boundary term of the action is dependent on the extrinsic curvature K, and since we are choosing to define the quantum gravity region as enclosed by intersecting hypersurfaces on which $K = 0$, this term also vanishes. The total gravitational action is solely dependent on the action at the corner of the quantum gravity region. Following [54], we showed that the corner term of the action may be written in terms of the boost angle η between the normals to the hypersurfaces at their intersection. The next step in our study is to find the geodesics describing the hypersurfaces that define the boundary of the quantum gravity region, and use these geodesics to determine the boost angle between the normals to the hypersurfaces. We deal with the calculation of the geodesics in the next chapter.

Chapter 5

Finding the Maximal Surfaces

In Chapter 4 we defined the 'quantum gravity region' of our spacetime as the region enclosed by the spacelike hypersurface on which the trace of the extrinsic curvature is zero ($K = 0$) and its time reversal, and we showed that the gravitational action for this spacetime is dependent only on the action at the corner of the quantum gravity region, S_C. Vanishing extrinsic curvature implies that the variation of the volume of the hypersurfaces is equal to zero [23, 85], and we will therefore refer to them as 'maximal surfaces' from this point onwards. In this section we show, following Christodoulou and De Lorenzo [23], that the problem of finding the maximal surfaces can be reduced to the solution of a 2-dimensional geodesic equation. We then deduce the maximal surfaces using three different coordinate systems: Eddington-Finkelstein, Schwarzschild and Kruskal.

The line element of a generic spherically symmetric spacetime is

$$\begin{aligned} \mathrm{d}s^2 &= g_{\mu\nu} dx^\mu \mathrm{d}x^\nu \\ &= g_{AB} \mathrm{d}x^A \mathrm{d}x^B + r^2 \mathrm{d}\Omega^2 \end{aligned} \tag{5.1}$$

where $\mu, \nu = \{0, 1, 2, 3\}$, $A, B = \{0, 1\}$ and $d\Omega^2 = d\theta^2 + \sin^2\theta d\phi^2$ is the metric on a unit 2-sphere. We choose coordinates $x^\mu = \{t, r, \theta, \phi\}$ and $x^A = \{t, r\}$. We decompose the hypersurfaces Σ into a curve γ and a 2-dimensional sphere:

$$\Sigma = \gamma \times \mathbb{S}^2. \tag{5.2}$$

Parameterizing γ by λ and choosing that γ lies in the $t - r$ plane we have

$$\gamma : \lambda \to (t(\lambda), r(\lambda)). \tag{5.3}$$

The coordinates describing the 2-sphere are θ and ϕ, and the intrinsic coordinates of Σ are $y^a = \{\lambda, \theta, \phi\}$. The line element on Σ is then

$$\begin{aligned} \mathrm{d}s^2_\Sigma &= h_{ab} \mathrm{d}y^a \mathrm{d}y^b \\ &= (g_{AB} \dot{x}^A \dot{x}^B) \mathrm{d}\lambda^2 + r^2 \mathrm{d}\Omega^2 \end{aligned} \tag{5.4}$$

where $h_{ab} = g_{\mu\nu} e^\mu_a e^\nu_b$ is the induced metric on the hypersurface Σ, and $e^\mu_a = \partial x^\mu / \partial x^a$ are tangent vectors in Σ. Equation 5.4 is the diagonal line element, with the dots denoting differentiation with respect to λ. The components of the induced metric are

$$h_{\lambda\lambda} = g_{AB} \dot{x}^A \dot{x}^B \tag{5.5a}$$

$$h_{\theta\theta} = r^2 \tag{5.5b}$$

$$h_{\phi\phi} = r^2 \sin^2\theta. \tag{5.5c}$$

We now try to compute the volume of the hypersurface Σ. This volume may be expressed as

$$V[\Sigma] = \int_\Sigma \mathrm{d}y^3 \sqrt{\det(h_{ab})} \tag{5.6}$$

where $\mathrm{d}y^3 = d\lambda d\theta d\psi$. Since h_{ab} is diagonal, we simply multiply Equations 5.5a-5.5c to find its determinant:

$$\det(h_{ab}) = (r^4 g_{AB} \dot{x}^A \dot{x}^B) \sin^2\theta. \tag{5.7}$$

The volume $V[\Sigma]$ is then

$$\begin{aligned} V[\Sigma] &= \int_\Sigma \sqrt{r^4 g_{AB} \dot{x}^A \dot{x}^B \sin^2\theta}\; d\lambda d\theta d\psi \\ &= \int_\gamma \sqrt{r^4 g_{AB} \dot{x}^A \dot{x}^B}\; d\lambda \cdot \int_{\mathbb{S}^2} \sin\theta\; d\theta d\psi \\ &= 4\pi \int_\gamma (\tilde{g}_{AB} \dot{x}^A \dot{x}^B)^{1/2}\; d\lambda \end{aligned} \tag{5.8}$$

where $\tilde{g}_{AB} = r^4 g_{AB}$ is a 2-dimensional auxiliary metric. Extremization of Equation 5.8 gives

$$\dot{x}^A \tilde{\nabla}_A \dot{x}^B = 0, \tag{5.9}$$

where $\tilde{\nabla}_A$ is the covariant derivative in $\tilde{g}_{AB}$. Since $A, B = (0, 1)$, Equation 5.9 is a 2-dimensional geodesic equation. Determination of the maximal surfaces has thus been reduced to the solution of a 2-dimensional geodesic problem.

5.1 Eddington-Finkelstein Coordinates

The Schwarzschild line element $ds^2 = -f(r)dt^2 + f^{-1}(r)dr^2 + r^2 d\Omega^2$ is a convenient choice for our spacetime because it is spherically symmetric. We use advanced time Eddington-Finkelstein coordinates (v, r) where

$$v = t + r^* \tag{5.10}$$

and $r^* = r + 2m \ln|r - 2m|$. In these coordinates the Schwarzschild line element becomes

$$\mathrm{d}s^2 = -f(r)\mathrm{d}v^2 + 2\mathrm{d}v\mathrm{d}r + r^2 \mathrm{d}\Omega^2, \tag{5.11}$$

and the line element on the hypersurface Σ is

$$ds^2_\Sigma = (-f(r)\dot{v}^2 + 2\dot{v}\dot{r})d\lambda^2 + r^2 d\Omega^2. \tag{5.12}$$

The spacelike condition on this line element is $-f(r)\dot{v}^2 + 2\dot{v}\dot{r} > 0$. The volume of Σ may then be expressed as

$$V[\Sigma] = 4\pi \int_\gamma \sqrt{r^4(-f(r)\dot{v}^2 + 2\dot{v}\dot{r})}\, d\lambda, \tag{5.13}$$

where the Lagrangian of a particle with motion described by the line element in Equation 5.12 is defined by

$$\mathcal{L}(v, r, \dot{v}, \dot{r}) = \sqrt{r^4(-f(r)\dot{v}^2 + 2\dot{v}\dot{r})}. \tag{5.14}$$

The 2-dimensional auxiliary line element is

$$d\tilde{s}^2 = r^4(-f(r)dr^2 + 2dvdr). \tag{5.15}$$

We now have enough information to deduce the geodesic equations, and thus define the $K = 0$ surfaces. We could use Equation 5.9, but this would require computation of Christoffel symbols. A simpler way to find the geodesics is to use conserved quantities. Our spacetime metric has a stationary symmetry given by the Killing vector:

$$\zeta = \partial_v = (1, 0). \tag{5.16}$$

We can therefore define our conserved quantity E as

$$\begin{aligned} E &= \tilde{g}_{AB}\zeta^A \dot{x}^B \\ &= \tilde{g}_{00}\zeta^0\dot{x}^0 + \tilde{g}_{01}\zeta^0\dot{x}^1 \\ &= -r^4 f(r)\dot{v} + r^4\dot{r} \\ \Rightarrow E &= r^4(-f(r)\dot{v} + \dot{r}). \end{aligned} \tag{5.17}$$

The geodesics will be defined by $\dot{v}$ and $\dot{r}$. Extremization of the volume of Σ is equivalent to finding the equations of motion corresponding to the Lagrangian (Equation 5.14). We take the normalization condition to be $\mathcal{L}(v, r, \dot{v}, \dot{r}) = r_s^3$, then

$$r^4(-f(r)\dot{v}^2 + 2\dot{v}\dot{r}) = r_s^6. \tag{5.18}$$

Equations 5.17 and 5.18 can then be solved simultaneously to find

$$\dot{r} = \pm r^{-4}\sqrt{E^2 + r_s^6 r^4 f(r)}. \tag{5.19}$$

Following Christodoulou [24], we choose $\dot{r}$ to be negative. This choice restricts us to the interior of the black hole region, and thus the resulting geodesics describing the maximal surfaces will only be valid in this region. In advanced time coordinates, the geodesics are

$$\dot{r} = -r^{-4}\sqrt{E^2 + r_s^6 r^4 f(r)} \tag{5.20a}$$

$$\dot{v} = \frac{r_s^6}{E + r^4\dot{r}}. \tag{5.20b}$$

We can repeat the above analysis using the retarded time Eddington-Finkelstein coordinates (u, r) where

$$u = t - r^* \tag{5.21}$$

and r^* is defined as in Equation 5.10. The resulting geodesics are

$$\dot{r} = r^{-4}\sqrt{E^2 + r_s^6 r^4 f(r)} \tag{5.22a}$$

$$\dot{u} = -\frac{r_s^6}{r^4\dot{r} - E}. \tag{5.22b}$$

Equations 5.20 and 5.22 define the maximal surfaces in retarded time coordinates.

5.2 Schwarzschild Coordinates

We now derive the geodesics defining the $K = 0$ surfaces using Schwarzschild coordinates in addition to the Eddington-Finkelstein coordinates used above. The full Schwarzschild line element is

$$ds^2 = -f(r)dt^2 + f(r)^{-1}dr^2 + r^2 d\Omega^2, \tag{5.23}$$

and the line element on the hypersurface is

$$ds_\Sigma^2 = (-f(r)\dot{t}^2 + f^{-1}(r)\dot{r}^2)d\lambda^2 + r^2 d\Omega^2. \tag{5.24}$$

In order for this hypersurface to be spacelike, we must have the expression inside the brackets in Equation 5.24 > 0 i.e. $-f(r)\dot{t}^2 + f^{-1}(r)\dot{r}^2 > 0$. The volume of the hypersurface may be expressed in the same way as in Equation 5.6:

$$V[\Sigma] = \int_\Sigma dy^3 \sqrt{\det(h_{ab})}. \tag{5.25}$$

The induced metric h_{ab} is diagonal, with components

$$h_{\lambda\lambda} = -f(r)\dot{t}^2 + f(r)^{-1}\dot{r}^2 \tag{5.26a}$$

$$h_{\theta\theta} = r^2 \tag{5.26b}$$

$$h_{\phi\phi} = r^2 \sin^2\theta. \tag{5.26c}$$

The volume is then

$$\begin{aligned} V[\Sigma] &= \int_\Sigma \sqrt{r^4 \sin^2\theta(-f(r)\dot{t}^2 + f(r)^{-1}\dot{r}^2)}\, d\lambda d\theta d\psi \\ &= \int_\gamma \sqrt{r^4(-f(r)\dot{t}^2 + f(r)^{-1}\dot{r}^2)}\, d\lambda \cdot \int_{\mathbb{S}} \sqrt{\sin^2\theta}\, d\theta d\psi \\ &= 4\pi \int_\gamma \sqrt{r^4(-f(r)\dot{t}^2 + f(r)^{-1}\dot{r}^2)}\, d\lambda, \end{aligned} \tag{5.27}$$

and the Lagrangian of a particle whose motion is described by the line element on the hypersurface is

$$\mathcal{L}(v, r, \dot{v}, \dot{r}) = \sqrt{r^4(-f(r)\dot{t}^2 + f^{-1}(r)\dot{r}^2)}. \tag{5.28}$$

Using the same approach as in Section 5.1, we set the Lagrangian equal to r_s^3, giving

$$\sqrt{r^4(-f(r)\dot{t}^2 + f^{-1}(r)\dot{r}^2)} = r_s^3. \tag{5.29}$$

Our conserved quantity E is defined by $E = \tilde{g}^{\text{Sch.}}_{AB}\zeta^A\dot{x}^B$ with Killing vector $\zeta = \partial_v = (1, 0)$. The auxiliary Schwarzschild metric is

$$\begin{aligned}\tilde{g}^{\text{Sch.}}_{AB} &= r^4 g_{AB} \\ &= \begin{pmatrix} -r^4 f(r) & 0 & 0 & 0 \\ 0 & r^4 f^{-1}(r) & 0 & 0 \\ 0 & 0 & r^6 & 0 \\ 0 & 0 & 0 & r^6 \sin^2\theta \end{pmatrix}.\end{aligned} \tag{5.30}$$

E is then

$$\begin{aligned} E &= \tilde{g}^{\text{Sch.}}_{AB}\zeta^A\dot{x}^B \\ &= \tilde{g}^{\text{Sch.}}_{00}\zeta^0\dot{x}^0 \\ &= -r^4 f(r)\dot{t} \end{aligned}$$

$$\Rightarrow E = -r^4 f(r)\dot{t}. \tag{5.31}$$

Solving Equations 5.29 and 5.31 simultaneously we find the geodesics defining the $K = 0$ surfaces to be

$$\dot{r} = \pm r^{-4}\sqrt{E^2 + r_s^6 r^4 f(r)} \tag{5.32a}$$

$$\dot{t} = -Er^{-4}f^{-1}(r). \tag{5.32b}$$

5.3 Kruskal Coordinates

To move from the Schwarzschild coordinates (t, r, θ, ϕ) to the Kruskal coordinates, we introduce a new timelike coordinate T and a new spacelike coordinate R such that our spacetime is described by (T, R, θ, ϕ). In terms of the (U, V) coordinates we defined in Chapter 2, these are

$$U = T - R \tag{5.33a}$$

$$V = T + R. \tag{5.33b}$$

The maximal surfaces in the (T, R) coordinates will be characterized by $\dot{T}$ and $\dot{R}$. T and R are defined by [17]

$$T = \left(\frac{r}{r_s} - 1\right)^{1/2} e^{r/2r_s} \sinh\left(\frac{t}{2r_s}\right) \tag{5.34a}$$

$$R = \left(\frac{r}{r_s} - 1\right)^{1/2} e^{r/2r_s} \cosh\left(\frac{t}{2r_s}\right) \tag{5.34b}$$

in the exterior region of the black hole $r > r_s$, and

$$T = \left(1 - \frac{r}{r_s}\right)^{1/2} e^{r/2r_s} \cosh\left(\frac{t}{2r_s}\right) \tag{5.35a}$$

$$R = \left(1 - \frac{r}{r_s}\right)^{1/2} e^{r/2r_s} \sinh\left(\frac{t}{2r_s}\right) \tag{5.35b}$$

in the interior region $r < r_s$. These definitions lead to the relations

$$\frac{t}{r_s} = 2\tanh^{-1}\left(\frac{T}{R}\right) \tag{5.36a}$$

$$\frac{t}{r_s} = 2\tanh^{-1}\left(\frac{R}{T}\right) \tag{5.36b}$$

where Equation 5.36a is valid outside the black hole, and Equation 5.36b is valid inside. On the union of the exterior region, the event horizon and the interior region, the Schwarzschild radial coordinate r is defined in terms of T and R as the solution of the equation

$$T^2 - R^2 = \left(1 - \frac{r}{r_s}\right) e^{r/r_s}. \tag{5.37}$$

The solution can be written as

$$r = r_s\left(1 + W_0\left(\frac{R^2 - T^2}{e}\right)\right) \tag{5.38}$$

where W_0 is the principal branch of the Lambert W function [26]. In the interior region $r < r_s$, we can deduce from Equation 5.37 that

$$0 < T^2 - R^2 < 1 \text{ and } T > 0. \tag{5.39}$$

Conversely, for the exterior region $r > r_s$ we have

$$T^2 - R^2 < 0 \text{ and } R > 0. \tag{5.40}$$

In the (T, R) coordinates, the Schwarzschild line element becomes

$$ds^2 = \frac{4r_s^3}{r} e^{-r/r_s}(-dT^2 + dR^2) + r^2 d\Omega^2, \tag{5.41}$$

and the auxiliary line element is

$$ds_\Sigma^2 = 4r^3 r_s^3 e^{-r/r_s}(dR^2 - dT^2). \tag{5.42}$$

Since the definitions of the Kruskal coordinates are dependent on whether we are inside or outside of the black hole, we must calculate the Killing vector for the interior and exterior regions separately (although we will find that the Killing vectors for both of these regions are in fact identical). In Schwarzschild coordinates, the Killing vector is $\zeta = \partial_t = (0, 1)$. In Kruskal coordinates, the Killing vector is defined by

$$\zeta = \partial_t = \frac{\partial}{\partial T}\frac{\partial T}{\partial t} + \frac{\partial}{\partial R}\frac{\partial R}{\partial t} = \partial_T \frac{\partial T}{\partial t} + \partial_R \frac{\partial R}{\partial t}. \tag{5.43}$$

Differentiating Equation 5.37 with respect to t gives a relation between $\frac{\partial T}{\partial t}$ and $\frac{\partial R}{\partial t}$ which holds for both the exterior and interior regions:

$$\begin{aligned} 2T\frac{\partial T}{\partial t} - 2R\frac{\partial R}{\partial t} &= 0 \\ \Rightarrow T\frac{\partial T}{\partial t} &= R\frac{\partial R}{\partial t}. \end{aligned} \tag{5.44}$$

We first deduce the Killing vector for the exterior region of the black hole. Rearranging Equation 5.36a we find that

$$\tanh\left(\frac{t}{2r_s}\right) = \frac{T}{R}. \tag{5.45}$$

Differentiating this equation with respect to t gives

$$\frac{\operatorname{sech}^2\left(\frac{t}{2r_s}\right)}{2r_s} = \frac{R\frac{\partial T}{\partial t} - T\frac{\partial R}{\partial t}}{R^2} \tag{5.46}$$

where on the right hand side we have used the quotient rule. Using the trigonometric identity $\operatorname{sech}^2\theta = 1 - \tanh^2\theta$, we can rewrite this as

$$\frac{1 - \frac{T^2}{R^2}}{2r_s} = \frac{R\frac{\partial T}{\partial t} - T\frac{\partial R}{\partial t}}{R^2}. \tag{5.47}$$

Solving the above equation simultaneously with Equation 5.44, we find expressions for $\frac{\partial T}{\partial t}$ and $\frac{\partial R}{\partial t}$ in terms of T and R:

$$\frac{\partial T}{\partial t} = \frac{R}{2r_s} \tag{5.48a}$$

$$\frac{\partial R}{\partial t} = \frac{T}{2r_s}. \tag{5.48b}$$

The Killing vector (Equation 5.43) for the exterior region of the black hole is then

$$\zeta = \frac{1}{2r_s}(R\partial_T + T\partial_R). \tag{5.49}$$

We now calculate the Killing vector for the interior region of the black hole. Rearranging Equation 5.36b gives

$$\tanh\left(\frac{t}{2r_s}\right) = \frac{R}{T}. \tag{5.50}$$

Differentiating this with respect to t leads to

$$\frac{\text{sech}^2\left(\frac{t}{2r_s}\right)}{2r_s} = \frac{T\frac{\partial R}{\partial t} - R\frac{\partial T}{\partial t}}{T^2} \tag{5.51}$$

$$\Rightarrow \frac{R^2 - T^2}{2r_s} = \frac{1}{T}\frac{\partial R}{\partial t}(R^2 - T^2) \tag{5.52}$$

where in the second line we used the relation between $\frac{\partial T}{\partial t}$ and $\frac{\partial R}{\partial t}$ (Equation 5.44). We find that

$$\frac{\partial T}{\partial t} = \frac{R}{2r_s} \tag{5.53a}$$

$$\text{and } \frac{\partial R}{\partial t} = \frac{T}{2r_s}, \tag{5.53b}$$

and the Killing vector for the interior region of the black hole is therefore identical to that of the exterior region:

$$\zeta = \frac{1}{2r_s}(R\partial_T + T\partial_R). \tag{5.54}$$

The conserved quantity associated to this Killing vector is

$$\begin{aligned} E &= \tilde{g}_{AB}\zeta^A\dot{x}^B \\ &= 2r^3r_s^2e^{-r/r_s}(T\dot{R} - \dot{T}R). \end{aligned} \tag{5.55}$$

We notice that the Lagrangian of a particle whose motion is described the by the line element in Equation 5.42 is

$$\mathcal{L} = 4r^3r_s^3e^{-r/r_s}(\dot{R}^2 - \dot{T}^2), \tag{5.56}$$

and we set this Lagrangian equal to r_s^6 (following the method in Sections 5.1 and 5.2) so that

$$4r^3r_s^3e^{-r/r_s}(\dot{R}^2 - \dot{T}^2) = r_s^6. \tag{5.57}$$

Equation 5.55 can be rearranged to find an expression for $\dot{R}$,

$$\dot{R} = \frac{1}{T}\left(\frac{Ee^{r/r_s}}{2r^3r_s^2} + R\dot{T}\right), \tag{5.58}$$

which describes one of the maximal surfaces. Substituting this into Equation 5.57, we obtain a quadratic equation in terms of $\dot{T}$:

$$\dot{T}^2(R^2 - T^2) + \frac{Ee^{r/r_s}}{r^3r_s^2}R\dot{T} + \frac{E^2e^{2r/r_s}}{4r^6r_s^4} - \frac{e^{r/r_s}r_s^3}{4r^3}T^2 = 0. \tag{5.59}$$

For notational simplicity we let

$$\alpha = R^2 - T^2 \tag{5.60a}$$

$$\beta = \frac{Ee^{r/r_s}}{r^3 r_s^2} R \tag{5.60b}$$

$$\text{and } \gamma = \frac{E^2 e^{2r/r_s}}{4r^6 r_s^4} - \frac{e^{r/r_s} r_s^2}{4r^3} T^2, \tag{5.60c}$$

then $\dot{T}$ is the solution of the quadratic formula

$$\dot{T} = \frac{-\beta \pm \sqrt{\beta^2 - 4\alpha\gamma}}{2\alpha}, \tag{5.61}$$

valid only when $\beta^2 - 4\alpha\gamma > 0$. Equations 5.58 and 5.61 characterize the maximal surfaces in the Kruskal coordinates. Now we have deduced expressions for the maximal surfaces, the next step is to calculate the boost angle between the normals to these surfaces.

5.4 Conclusion

In this chapter we derived the geodesics describing the maximal surfaces which define the boundary of the quantum gravity region. We first used Eddington-Finkelstein coordinates, and then repeated the calculation in both Schwarzschild and Kruskal coordinates. For each case, the geodesics were written in terms of the conserved quantity given by the stationary symmetry associated to the Killing vector of our spacetime. Now that we have characterized the maximal surfaces using geodesic equations, we may use these geodesics to find the boost angle between the normals to the maximal surfaces, and thus deduce the corner term of the gravitational action. Chapter 6 is concerned with the calculation of the boost angle.

Chapter 6

Computing the Boost Angle

In Chapter 5 we deduced the geodesics characterizing the maximal surfaces defining the quantum gravity region. The next step in our calculation is to use these geodesics to find the boost angle between the normals to the maximal surfaces, and thus the full gravitational action of our spacetime. Once we have an expression for the full gravitational action, we can approximate the black-to-white hole tunnelling amplitude.

6.1 Schwarzschild Coordinates

In Schwarzschild coordinates, the maximal surfaces are described by the geodesics

$$\dot{r} = \pm r^{-4}\sqrt{E^2 + r_s^6 r^4 f(r)} \tag{6.1a}$$

$$\dot{t} = -Er^{-4}f^{-1}(r) \tag{6.1b}$$

as shown in Section 5.2. $E = -r^4 f(r)\dot{t}$ is a conserved quantity along the geodesics. E will be either E_1 or E_2 depending on whether the maximal surface has a positive or negative gradient.

To compute the normal covector n_μ to the maximal surfaces, we use two facts:

1. Tangent vectors $\dot{x}^\mu$ are orthogonal to the normals, i.e. $\dot{x}^\mu n_\mu = 0\ \forall \dot{x}$.
2. Since the maximal surfaces are spacelike, the normals to them are timelike i.e. $n_\mu n^\mu = -1$.

Assume that we have coordinates $x^\mu = (t, r, \theta, \psi)$, then

$$\begin{aligned}\dot{x}^\mu &= (\dot{t}, \dot{r}, \dot{\theta}, \dot{\psi}) \\ &= (\dot{t}, \dot{r}, 0, 0)\end{aligned} \tag{6.2}$$

where the last line follows from the spherical symmetry of our spacetime. Since we are in the (r,t)-plane we choose the normal covector to be $n_\mu = (a, b, 0, 0)$. The timelike condition (2) can be written as

$$g^{\mu\nu} n_\mu n_\nu = -1 \tag{6.3}$$

where $g^{\mu\nu}$ is the inverse Schwarzschild metric

$$g^{\mu\nu} = \text{diag}(-f^{-1}(r), f(r), r^{-2}, (r\sin\theta)^{-2}) \tag{6.4}$$

$$\Rightarrow -f^{-1}(r)a^2 + f(r)b^2 = -1. \tag{6.5}$$

Condition 1 gives

$$\dot{x}^\mu n_\mu = a\dot{t} + b\dot{r} = 0$$
$$\Rightarrow a = -\frac{b\dot{r}}{\dot{t}}.$$

Substituting this expression for a into Equation 6.5 gives

$$-f^{-1}(r)\frac{b^2\dot{r}^2}{\dot{t}^2} + f(r)b^2 = -1. \tag{6.6}$$

We can then use the expressions for $\dot{r}$ and $\dot{t}$ in Equations 6.1a and 6.1b to deduce that

$$b = \pm E r_s^{-3} r^{-2} f^{-1}(r)$$
$$\Rightarrow a = \pm r_s^{-3} r^{-2}\sqrt{E^2 + r_s^6 r^4 f(r)}.$$

We consider the maximal surface with positive gradient, Σ_0. For this surface we have

$$n_\mu = \left(\epsilon_0 r_s^{-3} r^{-2}\sqrt{E_2^2 + r_s^6 r^4 f(r)}, \epsilon_0' E_2 r_s^{-3} r^{-2} f^{-1}(r), 0, 0\right) \tag{6.7}$$

and

$$n^\mu = g^{\mu\nu} n_\nu = \left(-\epsilon_0 r_s^{-3} r^{-2} f^{-1}(r)\sqrt{E_2^2 + r^4 f(r)}, \epsilon_0' E_2 r_s^{-3} r^{-2}, 0, 0\right) \tag{6.8}$$

where we have used the inverse Schwarzschild metric $g^{\mu\nu}$ (Equation 6.4) to calculate n^μ. The definition of ϵ_0 is dependent on whether we are looking inside or outside of the black hole horizon:

- $\epsilon_0 = +1$ when $r > r_s$, since $f(r) > 0$ in this region.
- $\epsilon_0 = -1$ when $r < r_s$, since $f(r) < 0$ in this region.
- $\epsilon_0' = +1\ \forall r$.

We assume that the conserved quantities E_1 and E_2 are associated to the gradients of the maximal surfaces, so that $E_2 > 0$ for the surface Σ_0. For Σ_1, we instead have

$$n'_\mu = \left(\epsilon_1 r_s^{-3} r^{-2}\sqrt{E_1^2 + r_s^6 r^4 f(r)}, \epsilon_1' E_1 r_s^{-3} r^{-2} f^{-1}(r), 0, 0\right). \tag{6.9}$$

and

$$n'^\mu = g^{\mu\nu} n_\nu = \left(-\epsilon_1 r_s^{-3} r^{-2} f^{-1}(r)\sqrt{E_1^2 + r^4 f(r)}, \epsilon_1' E_1 r_s^{-3} r^{-2}, 0, 0\right) \tag{6.10}$$

where $E_1 < 0$ and ϵ_1 is defined in a similar way to ϵ_0:

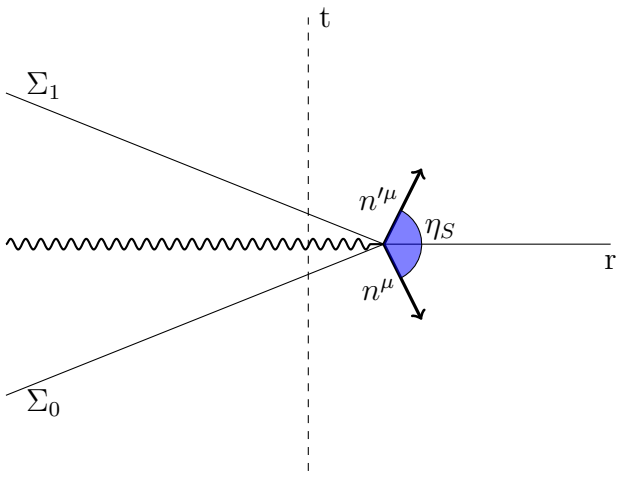

Figure 6.1: The (r, t) plane with the maximal surfaces Σ_0 and Σ_1. The angle between Σ_0 and Σ_1 is η_S. n^μ and n'^μ are the normal vectors to Σ_0 and Σ_1 respectively.

- $\epsilon_1 = -1$ when $r > r_s$.
- $\epsilon_1 = +1$ when $r < r_s$.
- $\epsilon_1' = -1\ \forall r$.

Figure 6.1 shows the (r, t)-plane with the maximal surfaces Σ_0 and Σ_1. η_S is the angle between the maximal surfaces. The subscript S serves as a reminder that we are working in the Schwarzschild coordinates, and the expression for the boost angle is dependent on the chosen coordinate system. η^μ and η'^μ are the normal vectors to Σ_0 and Σ_1 respectively. η_S is defined in terms of the normal vectors as follows:

$$\cosh \eta_S = -n'_\mu n^\mu. \tag{6.11}$$

$\cosh \eta_S$ is therefore

$$\cosh \eta_S = -r_s^{-6} r^{-4} f^{-1}(r) \Big(- \epsilon_1 \epsilon_0 \sqrt{E_1^2 + r_s^6 r^4 f(r)} \sqrt{E_2^2 + r_s^6 r^4 f(r)} + \epsilon_1' \epsilon_0' E_1 E_2 \Big). \tag{6.12}$$

Using the definitions of ϵ_0 and ϵ_1 above, we find that $-\epsilon_1 \epsilon_0 = 1$ for both $r > r_s$ and $r < r_s$, and $\epsilon_1' \epsilon_0' = -1\ \forall r$. The boost angle η_S for both the exterior and interior regions of the black hole is therefore given by the same expression:

$$\cosh \eta_S = -r_s^{-6} r^{-4} f^{-1}(r) \Big(\sqrt{E_1^2 + r_s^6 r^4 f(r)} \sqrt{E_2^2 + r_s^6 r^4 f(r)} - E_1 E_2 \Big). \tag{6.13}$$

Figure 6.2 is a MATLAB plot of the boost angle as given by Equation 6.13, as a function of r. The blue line is the real part of η_S, and the magenta line is the imaginary part. To produce this plot, we set $r_s = 1$, $E_1 = -2$ and $E_2 = 2$. The radial coordinate r is an array of linearly spaced points between 0 and 5, with the number of points $N = 10^5$. Inside the black hole horizon, i.e. $r_s < 1$, the boost angle is zero. Outside the horizon, $r_s > 1$,

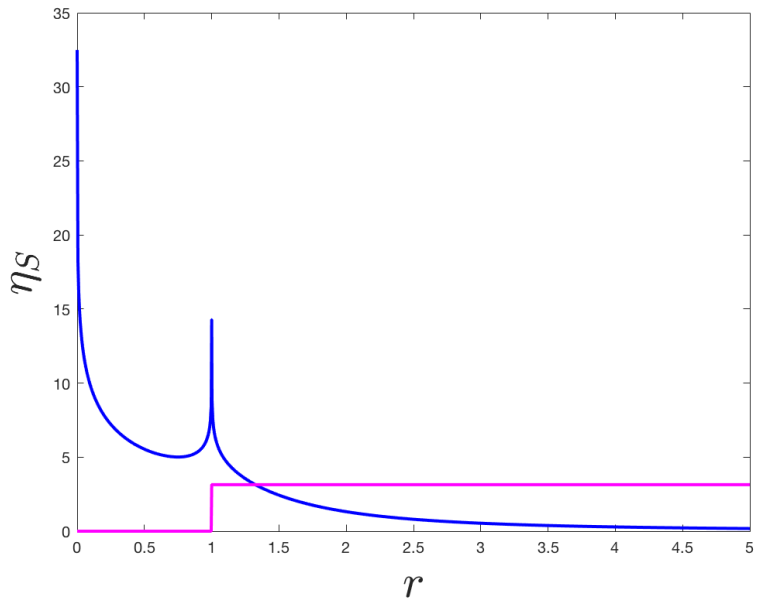

Figure 6.2: The boost angle η_S in Schwarzschild coordinates, plotted as a function of the radial coordinate r. The blue line is the real part of η_S, and the magenta line is the imaginary part. The Schwarzschild radius $r_s = 1$, and the conserved quantities are set to $E_1 = -2$ and $E_2 = 2$.

the boost angle has a constant imaginary part $i\pi$. In the region of spacetime in which quantum tunnelling occurs, we expect the gravitational action (and thus the boost angle) to have a finite imaginary part. On the horizon $r_s = 1$, there is a coordinate singularity and the real part of the boost angle is infinite. The reason for this coordinate singularity is made clear if we look at Equation 6.13: when $r = r_s$, $f(r) = 1 - \frac{r_s}{r} = 0$, and $f^{-1}(r)$ is therefore infinite. Since $\cosh^{-1}(\infty) = \infty$, the boost angle η_S is infinite on the horizon when expressed in Schwarzschild coordinates. In order to avoid this singularity, we may instead compute the boost angle in Kruskal coordinates. In these coordinates the boost angle is well-defined at the horizon.

6.2 Kruskal Coordinates

In Chapter 5, we deduced that in Kruskal coordinates, the maximal surfaces are defined by the geodesics

$$\dot{R} = \frac{1}{T}\left(\frac{Ee^{r/r_s}}{2r^3 r_s^2} + R\dot{T}\right) \tag{6.14a}$$

$$\text{and } \dot{T} = \frac{-\beta \pm \sqrt{\beta^2 - 4\alpha\gamma}}{2\alpha}, \tag{6.14b}$$

where

$$\alpha = R^2 - T^2 \tag{6.15a}$$

$$\beta = \frac{Ee^{r/r_s}}{r^3 r_s^2} R \tag{6.15b}$$

$$\text{and } \gamma = \frac{E^2 e^{2r/r_s}}{4r^6 r_s^4} - \frac{e^{r/r_s} r_s^3}{4r^3} T^2. \tag{6.15c}$$

For the derivation of these geodesics, see Section 5.3. We choose to work in the $R-T$ plane, so the tangent vectors to the surfaces defined in Equations 6.14a and 6.14b are $\dot{x}_\mu = (\dot{T}, \dot{R}, 0, 0)$. We denote the normal covectors to the maximal surfaces by $n_\mu = (A, B, 0, 0)$ where A and B are yet to be determined. To compute the normal covectors n_μ, we use the same approach as in Section 6.1. The two conditions to be satisfied are:

1. Tangent vectors $\dot{x}^\mu$ are orthogonal to the normals, i.e. $\dot{x}^\mu n_\mu = 0 \; \forall \dot{x}$.
2. Since the maximal surfaces are spacelike, the normals to them are timelike i.e. $n_\mu n^\mu = -1$.

The first condition gives

$$A\dot{T} + B\dot{R} = 0, \tag{6.16}$$

and the second gives

$$-A^2 + B^2 = -\frac{4r_s^3}{r} e^{-r/r_s}. \tag{6.17}$$

Solving the above two equations simultaneously and using Equation 5.57 to simplify the expression for B, we find

$$A = -\frac{B\dot{R}}{\dot{T}} \tag{6.18a}$$

$$B = \pm 4re^{-r/r_s}\dot{T}. \tag{6.18b}$$

On the union of the exterior region, the event horizon and the interior region of the black hole, the Kruskal coordinates (R, T) are related to the Schwarzschild radial coordinate r by

$$T^2 - R^2 = \left(1 - \frac{r}{r_s}\right) e^{r/r_s}. \tag{6.19}$$

Recall that outside the black hole horizon we have $r > r_s$, therefore $(1 - \frac{r}{r_s}) < 0$ and

$$T^2 - R^2 < 0 \text{ and } R > 0. \tag{6.20}$$

Conversely, for the interior region of the black hole we have

$$0 < T^2 - R^2 < 1 \text{ and } T > 0. \tag{6.21}$$

We would like to compute the boost angle η_K in the interior region. It is as yet unclear whether we should choose the positive or negative signs in Equations 6.14b and 6.18b. For the purpose of producing some preliminary plots, we choose the positive signs such that

$$\dot{T} = \frac{-\beta + \sqrt{\beta^2 - 4\alpha\gamma}}{2\alpha} \tag{6.22a}$$

$$\text{and } B = 4re^{-r/r_s}\dot{T} \tag{6.22b}$$

The normal covector n'_μ is given by

$$n'_\mu = \left(-B_1 \frac{\dot{R}_1}{\dot{T}_1}, B_1, 0, 0 \right) \tag{6.23}$$

where the subscript 1 corresponds to the conserved quantity E_1. We choose to interpret the conserved quantities E_1 and E_2 as the gradients of the maximal surfaces, so that $E_1 < 0$ and $E_2 > 0$. For now we assume that our quantum gravity region is symmetric and therefore $|E_1| = |E_2|$. For the second maximal surface we have

$$n_\mu = \left(-B_2 \frac{\dot{R}_2}{\dot{T}_2}, B_2, 0, 0 \right) \tag{6.24}$$

where the subscript 2 corresponds to the conserved quantity $E_2 > 0$. The boost angle η_K in the Kruskal coordinates is defined in the same way as in the Schwarzschild coordinates: $\cosh \eta_K = -n'_\mu n^\mu$. To calculate n^μ, we recall the full line element in the Kruskal coordinates:

$$ds^2 = \frac{4r_s^3}{r} e^{-r/r_s}(-dT^2 + dR^2) + r^2 d\Omega^2. \tag{6.25}$$

n^μ is then

$$n^\mu = g^{\mu\nu} n_\nu = \frac{e^{r/r_s} r}{4r_s^3}(-1, 1, 0, 0) \cdot \left(-B_2 \frac{\dot{R}_2}{\dot{T}_2}, B_2, 0, 0 \right) \tag{6.26}$$

$$= \frac{e^{r/r_s} r}{4r_s^3} \left(B_2 \frac{\dot{R}_2}{\dot{T}_2}, B_2, 0, 0 \right). \tag{6.27}$$

We now have all the information required to calculate the boost angle in Kruskal coordinates η_K:

$$\begin{aligned}
\cosh\eta_K &= -n'_\mu n^\mu = -\left(-B_1\frac{\dot{R}_1}{\dot{T}_1}, B_1, 0, 0\right)\cdot\frac{e^{r/r_s}r}{4r_s^3}\left(B_2\frac{\dot{R}_2}{\dot{T}_2}, B_2, 0, 0\right) \\
&= -\frac{e^{r/r_s}r}{4r_s^3}\left(-B_1\frac{\dot{R}_1}{\dot{T}_1}, B_1, 0, 0\right)\cdot\left(B_2\frac{\dot{R}_2}{\dot{T}_2}, B_2, 0, 0\right) \\
&= -\frac{e^{r/r_s}r}{4r_s^3}\left(-B_1B_2\frac{\dot{R}_1\dot{R}_2}{\dot{T}_1\dot{T}_2} + B_1B_2\right) \\
&= -\frac{B_1B_2e^{r/r_s}r}{4r_s^3}\left(1-\frac{\dot{R}_1\dot{R}_2}{\dot{T}_1\dot{T}_2}\right) \\
\Rightarrow \cosh\eta_K &= -\frac{B_1B_2e^{r/r_s}r}{4r_s^3}\left(1-\frac{\dot{R}_1\dot{R}_2}{\dot{T}_1\dot{T}_2}\right).
\end{aligned} \tag{6.28}$$

Equation 6.28 defines the boost angle η_K in terms of the geodesics $\dot{R}$ and $\dot{T}$. This expression is valid for all regions of our spacetime, subject to different conditions on R and T. In order to investigate the behaviour of the boost angle, we will plot Equation 6.28 using the programming language MATLAB for a range of (R, T) values.

6.2.1 The Interior Region

Figure 6.3 is a MATLAB plot of the real part of η_K in the interior region of the black hole as a function of the Kruskal coordinates (R, T). In order to produce this plot, we used the expression for η_K derived above (Equation 6.28) and imposed the conditions on R and T in the interior region: $0 < T^2 - R^2 < 1$ and $T > 0$ (Equation 6.21). R is 10^3 linearly spaced values between -2 and 2, and T is 10^3 linearly spaced values between 0 and 2. The Schwarzschild radius is set to $r_s = 1$ and the conserved quantities are chosen to be $E_1 = -2$, $E_2 = 2$. A two-dimensional view of Figure 6.28 in the (R, T)-plane is shown in Figure 6.4. It is clear from these figures that the real part of η_K is dependent on both R and T, as is expected. The plot diverges as we approach the hyperbola $T^2 - R^2 = 1$. This divergence makes physical sense if we consider the relation between the Kruskal and Schwarzschild coordinates, Equation 6.19. When $T^2 - R^2 = 1$, we have $\left(1 - \frac{r}{r_s}\right)e^{r/r_s} = 1$ and thus $r_s = 0$. The hyperbola $T^2 - R^2 = 1$ therefore corresponds to the central Schwarzschild singularity $r_s = 0$. There is another divergence in Figure 6.3 at $T = R = 0$. This divergence occurs because when $T = R$, $\alpha = R^2 - T^2 = 0$ which results in a factor of $\frac{1}{0}$ in the equation for $\dot{T}$ (Equation 6.14b). We note that neither of the divergences described above present an issue in our calculations, since they are in fact outside the validity of the Kruskal coordinates inside the black hole horizon (Equation 6.21). An important feature of Figure 6.3 is that the boost angle appears to be heavily damped in all regions of the spacetime except for in the vicinity of the black hole horizon at $T = \pm R$. We expect the quantum tunnelling transition to a white hole to take place near the horizon. Since we know that the probability

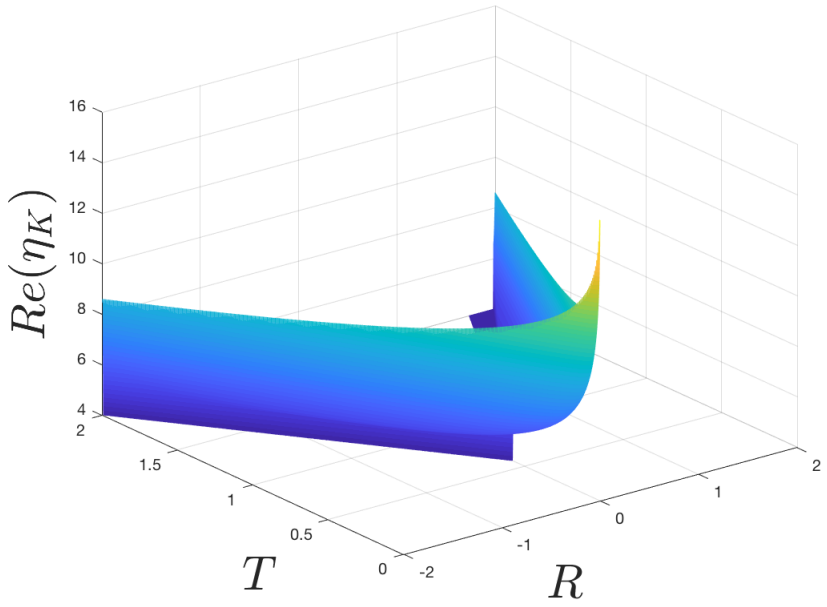

Figure 6.3: The real part of η_K in the interior region of the black hole. η_K is plotted in MATLAB as a function of the Kruskal coordinates R and T, where R is set to 10^3 linearly spaced values between -2 and 2 and T is 10^3 linearly spaced values between 0 and 2. The Schwarzschild radius is set to $r_s = 1$ and the conserved quantities are $E_1 = -2$, $E_2 = 2$.

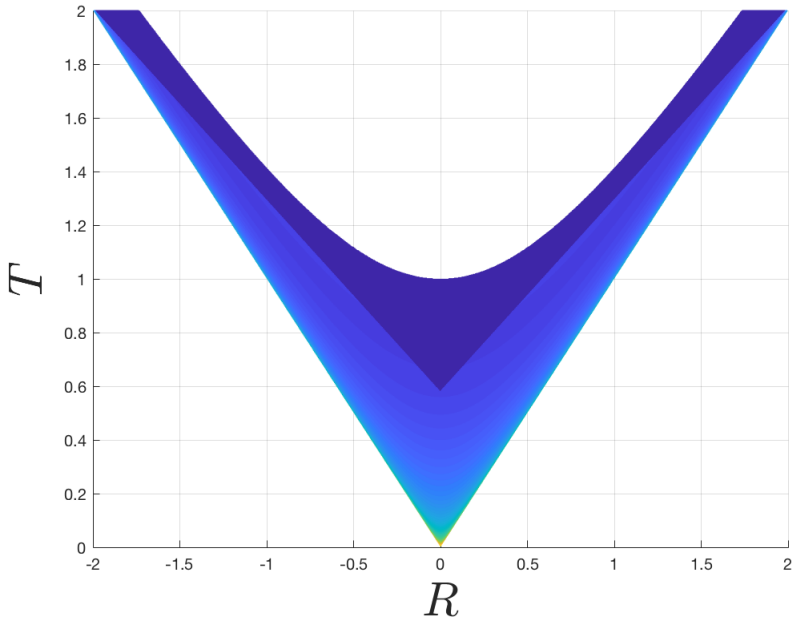

Figure 6.4: A two-dimensional view of Figure 6.3 in the (R, T)-plane. The boost angle η_K is dependent on both R and T. The lighter the shade of blue, the higher the value of η_K.

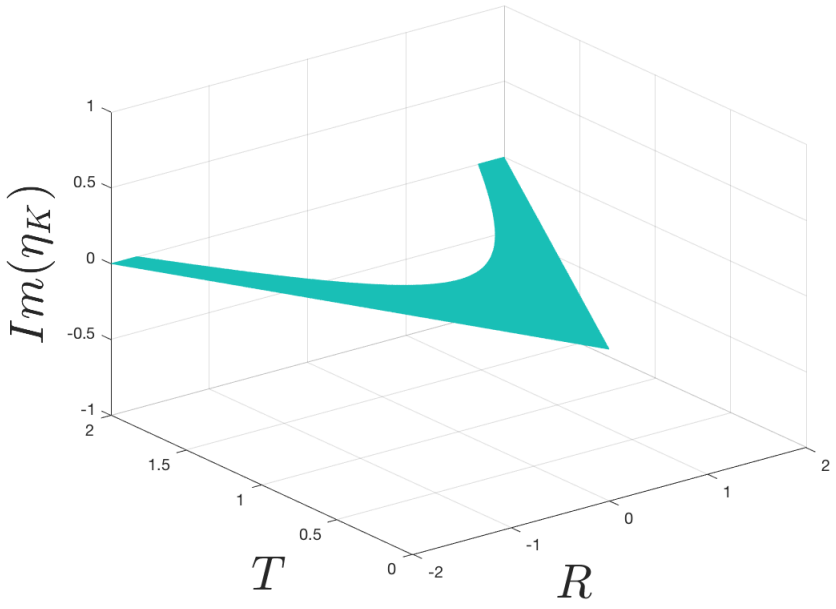

Figure 6.5: The imaginary part of η_K in the interior region of the black hole, corresponding to the real part in Figure 6.3.

of tunnelling is proportional to the value of the boost angle on the corner of the quantum gravity region, it makes intuitive sense for the value of η_K to increase as we approach the horizon. Figure 6.5 depicts the imaginary part of η_K in the interior region of the black hole. For the chosen values of $r_s = 1$, $E_1 = -2$ and $E_2 = 2$, the imaginary part of the boost angle is zero in the entire interior region of the black hole.

6.2.2 The Exterior Region

We also plot the boost angle for the exterior region of the black hole, where $r > r_s$. To do this, we use Equation 6.28 and implement the conditions on R and T for the exterior region: $T^2 - R^2 < 0$ and $R > 0$ (Equation 6.20). Figure 6.6 is a plot of the real part of η_K as a function of R and T for the exterior region with $r_s = 1$, $E_1 = -2$ and $E_2 = 2$. The value of $Re(\eta_K)$ is zero far from the horizon. Similarly to the plot of η_K in the interior region, there is a divergence at $T = R = 0$ because a factor of $\frac{1}{0}$ arises in the equation for $\dot{T}$ when R and T are equal. This divergence is irrelevant because the boundary $T = R$ is not included in the exterior region. As we move towards the horizon, $Re(\eta_K)$ increases to reach a maximum finite value close to the $T = R$ boundary. This maximum value approximately matches the value of $Re(\eta_K)$ near the horizon obtained by plotting the interior solution (≈ 9). This seems to suggest that the real part of the boost angle might be continuous across the horizon. We will check whether this is indeed the case by analysing the expression for η_K when $r = r_s$ and $T^2 = R^2$ (see Section 6.2.3). Figure 6.8 shows the imaginary part of the boost angle in the exterior region of the black hole. There

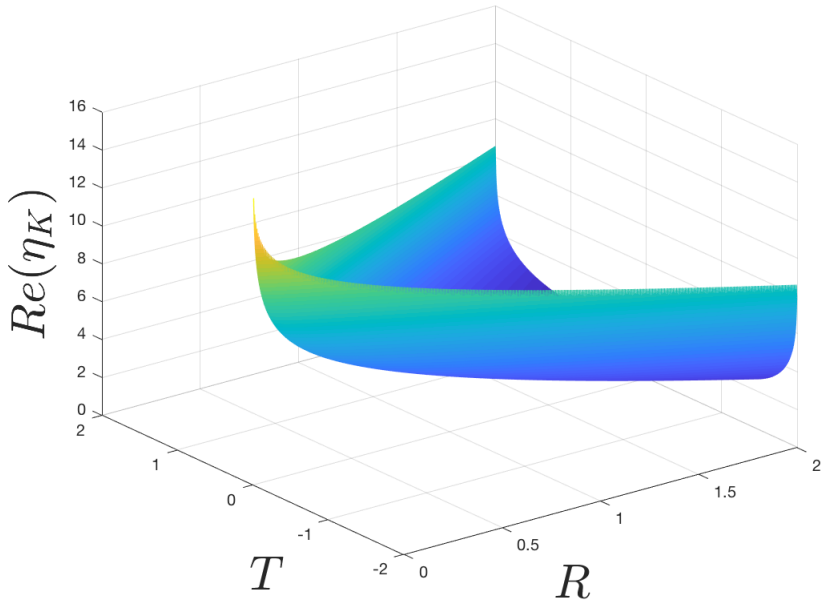

Figure 6.6: The real part of the boost angle η_K as a function of R and T for the exterior region of the black hole. We choose $r_s = 1$, $E_1 = -2$ and $E_2 = 2$.

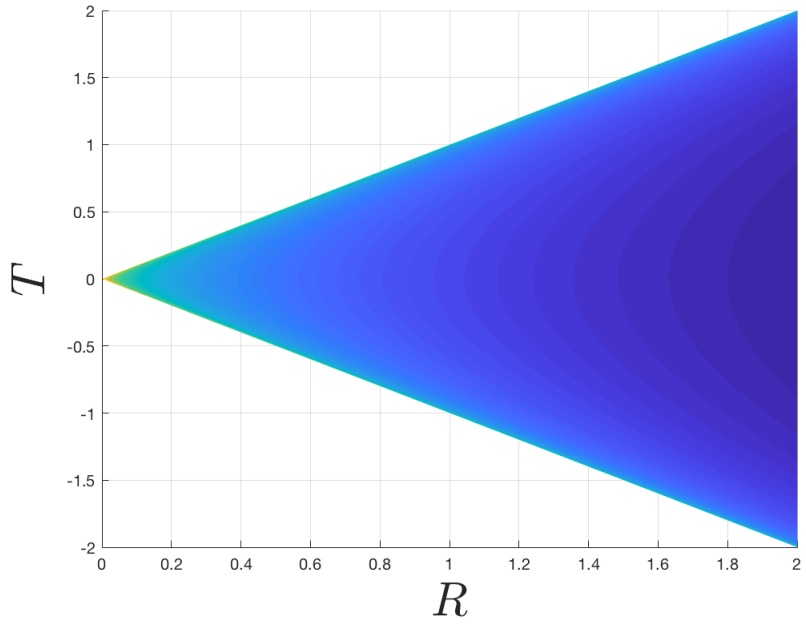

Figure 6.7: A two-dimensional view of Figure 6.6 in the (R, T)-plane.

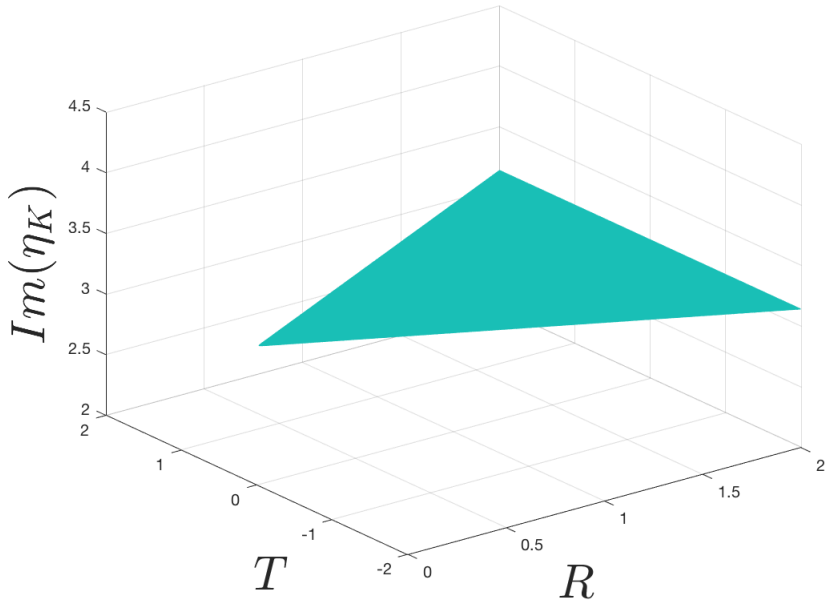

Figure 6.8: The imaginary part of η_K as a function of R and T in the exterior region of the black hole.

is a constant imaginary part of $i\pi$ everywhere outside the horizon ($r > r_s$). This result is in agreement with the result obtained using Schwarzschild coordinates (see Section 6.1).

6.2.3 On the Horizon

To check whether the boost angle is continuous through the black hole horizon, we must examine the expression for η_K where $r = r_s$ and $T = \pm R$. Equation 6.28 defines the boost angle in Kruskal coordinates for the interior and exterior regions of the black hole. When $r = r_s$, Equation 6.28 simplifies to

$$\cosh \eta_K = -\frac{B_1 B_2 e}{4r_s^2}\left(1 - \frac{\dot{R}_1 \dot{R}_2}{\dot{T}_1 \dot{T}_2}\right). \tag{6.29}$$

To simplify this further, we can substitute in the expressions for B_1, B_2, $\dot{R}_1$, $\dot{R}_2$, $\dot{T}_1$ and $\dot{T}_2$ and write η_K as a function of the Kruskal coordinates R and T only. As per Section 6.2, B_1 and B_2 are defined by

$$B_1 = 4r_s e^{-1}\dot{T}_1 \tag{6.30a}$$

$$B_2 = 4r_s e^{-1}\dot{T}_2. \tag{6.30b}$$

where we have provisionally chosen the positive signs for the purpose of plotting. Substituting these expressions into Equation 6.29 results in

$$\cosh \eta_K = -4e^{-1}\dot{T}_1\dot{T}_2 + 4e^{-1}\dot{R}_1\dot{R}_2. \tag{6.31}$$

Setting $r = r_s$ in the equation for $\dot{R}$ (Equation 6.14a), we have

$$\dot{R}_1 = \frac{1}{T}\left(\frac{E_1 e}{2r_s^5} + R\dot{T}_1\right) \tag{6.32a}$$

$$\text{and } \dot{R}_2 = \frac{1}{T}\left(\frac{E_2 e}{2r_s^5} + R\dot{T}_2\right). \tag{6.32b}$$

The relation between Schwarzschild and Kruskal coordinates, Equation 6.19, simplifies to

$$\begin{aligned} T^2 - R^2 &= 0 \\ \Rightarrow T &= \pm R, \end{aligned} \tag{6.33}$$

so in Kruskal coordinates the horizon is characterized by the surfaces $T = \pm R$. We will treat the surfaces $T = +R$ and $T = -R$ separately. Substituting Equation 6.33 into Equations 6.32a and 6.32b, we find

$$\dot{R}_1 = \pm\frac{1}{R}\left(\frac{E_1 e}{2r_s^5} + R\dot{T}_1\right) \tag{6.34a}$$

$$\text{and } \dot{R}_2 = \pm\frac{1}{R}\left(\frac{E_2 e}{2r_s^5} + R\dot{T}_2\right). \tag{6.34b}$$

As shown in Section 5.3, $\dot{T}$ is given by the solution of the quadratic equation

$$\dot{T}^2(R^2 - T^2) + \frac{Ee^{r/r_s}}{r^3 r_s^2}R\dot{T} + \frac{E^2 e^{2r/r_s}}{4r^6 r_s^4} - \frac{e^{r/r_s} r_s^3}{4r^3}T^2 = 0. \tag{6.35}$$

On the horizon we have $r = r_s$ and $T^2 = R^2$, so the above equation simplifies to

$$\frac{EeR}{r_s^5}\dot{T} + \frac{E^2 e^2}{4r_s^{10}} - \frac{eR^2}{4} = 0 \tag{6.36}$$

which is linear. Solving for $\dot{T}$ we find

$$\begin{aligned} \frac{EeR}{r_s^5}\dot{T} &= \frac{eR^2}{4} - \frac{E^2 e^2}{4r_s^{10}} \\ \Rightarrow \dot{T} &= \frac{r_s^5}{EeR}\left(\frac{eR^2}{4} - \frac{E^2 e^2}{4r_s^{10}}\right) \\ \Rightarrow \dot{T} &= \frac{R^2 r_s^{10} - E^2 e}{4ERr_s^5}. \end{aligned} \tag{6.37}$$

$\dot{T}_1$ and $\dot{T}_2$ are therefore defined by

$$\dot{T}_1 = \frac{R^2 r_s^{10} - E_1^2 e}{4E_1 R r_s^5} \tag{6.38a}$$

$$\text{and } \dot{T}_2 = \frac{R^2 r_s^{10} - E_2^2 e}{4E_2 R r_s^5}. \tag{6.38b}$$

We will first consider the positive branch, $T = +R$. Substituting Equations 6.34 and 6.38 into Equation 6.31 results in

$$\begin{aligned}\cosh \eta_K = &-4e^{-1}\left(\frac{R^2 r_s^{10} - E_1^2 e}{4E_1 R r_s^5}\right)\left(\frac{R^2 r_s^{10} - E_2^2 e}{4E_2 R r_s^5}\right) \\ &+ \frac{4e^{-1}}{R^2}\left(\frac{E_1 e}{2r_s^5} + \frac{R^2 r_s^{10} - E_1^2 e}{4E_1 r_s^5}\right)\left(\frac{E_2 e}{2r_s^5} + \frac{R^2 r_s^{10} - E_2^2 e}{4E_2 r_s^5}\right)\end{aligned} \tag{6.39}$$

where we have chosen the positive signs in Equation 6.34. Writing the above equation in its simplest form requires some algebraic manipulation; for details see Appendix B. We find that Equation 6.39 reduces to an expression in terms of the conserved quantities E_1 and E_2 which is independent of the Kruskal coordinates R and T:

$$\cosh \eta_K = \frac{1}{2}\left(\frac{E_1}{E_2} + \frac{E_2}{E_1}\right). \tag{6.40}$$

We now consider the negative branch, $T = -R$. Substituting Equations 6.34 and 6.38 into Equation 6.31 with the negative signs chosen in Equation 6.34 results in the same expression as for the positive branch (Equation 6.39), since the two negative signs in $\dot{R}_1$ and $\dot{R}_2$ cancel each other out. We may therefore say that for the sign choices we have made, Equation 6.40 is valid for the entire region of the black hole horizon. We note that the two equations in 6.34 need not necessarily have the same sign. The case where $\dot{R}_1$ and $\dot{R}_2$ have different signs has not been explored in this thesis, but it is an important area for future study. Similarly, it is possible that the signs of $\dot{T}_1$ and $\dot{T}_2$ are not the same. In order to produce the preliminary plots above, we have made further assumptions concerning the values of the conserved quantities E_1 and E_2. Since E_1 and E_2 characterize the maximal surfaces and we know that the gradients of the maximal surfaces Σ_0 and Σ_1 will be opposite in sign, we let $E_1 = -E_2$. This is a simplification because E_1 and E_2 are not necessarily equal to the gradients of Σ_0 and Σ_1. For simplicity we also let $|E_1| = |E_2|$. Under these two conditions, Equation 6.40 will reduce to

$$\cosh \eta_K = -1 \tag{6.41}$$

$$\Rightarrow \eta_K = i\pi. \tag{6.42}$$

The above equation suggests that on the black hole horizon, the real part of the boost angle is zero and the imaginary part is $i\pi$. This result is surprising, since the real part of the boost angle approaches a finite positive value (≈ 9 for $r_s = 2$, $E_1 = -1$ and $E_2 = 2$) near the horizon (see Figures 6.3 and 6.6). A real part of zero on the horizon would therefore mean that the boost angle is discontinuous across the horizon, contrary to what we expect when working in the Kruskal coordinates. This could suggest that the values we have chosen for E_1 and E_2 are not appropriate. Further work is needed to choose these values correctly.

6.3 Tunnelling Amplitude

We have now deduced expressions for the boost angle η_K in the three distinct spacetime regions: the interior of the black hole, the exterior and on the horizon. We have found that for a particular choice of r_s and the conserved quantities E_1 and E_2, the real part of the boost angle tends towards a finite positive value as it approaches the horizon from either side. As discussed in Chapter 4, the probability that a black hole will quantum tunnel into a white hole is proportional to the gravitational action, which in our case reduces to the action at the corner of the quantum gravity region:

$$S = S_C = 4\pi r^2 \eta. \tag{6.43}$$

where r is the radius of the corner. The value of the gravitational action, and thus the tunnelling amplitude A of the quantum transition, clearly depends on the location of the corner of the quantum gravity region (the intersection of the maximal surfaces). We expect that the corner is in the vicinity of the black hole horizon, but it is not yet clear whether is is just inside the horizon, just outside or exactly on the horizon. For the first two cases we have

$$A \sim e^{iS_C} \sim \exp\left\{ i \cosh^{-1}\left(-\frac{B_1 B_2 e^{r/r_s} r}{4r_s^3}\left(1 - \frac{\dot{R}_1 \dot{R}_2}{\dot{T}_1 \dot{T}_2}\right)\right)\right\} \tag{6.44}$$

where A is the tunnelling amplitude and the Bs, $\dot{R}$s and $\dot{T}$s are defined in Section 6.2. If the corner is instead located on the horizon, the above expression simplifies to

$$A \sim e^{iS_C} \sim \exp\left\{ i \cosh^{-1}\left(\frac{1}{2}\left(\frac{E_1}{E_2} + \frac{E_2}{E_1}\right)\right)\right\} \tag{6.45}$$

or

$$A \sim e^{iS_C} \sim \left\{ i \cosh^{-1}(-1)\right\} = -\pi \tag{6.46}$$

if we assume, as in Section 6.2.3, that $|E_1| = |E_2|$. It does not make intuitive sense for the tunnelling amplitude to be purely real, or to be independent of the maximal surfaces defining the quantum gravity region. We can therefore conclude that Equation 6.46 is incorrect; perhaps the corner is located a small distance away from the black hole horizon rather than directly on it. Alternatively, it might not make sense to make the simplification that the conserved quantities associated to the maximal surfaces (E_1 and E_2) have equal magnitude. These are open questions that we will discuss further in Chapter 7.

6.4 Conclusion

In this chapter we computed the boost angle η between the normals to the maximal surfaces defining the boundary of the quantum gravity region. We first performed this calculation using Schwarzschild coordinates and found that the imaginary part of η is zero in the interior of the black hole, and has a constant value of $i\pi$ in the exterior region.

On the horizon $r = r_s$, there is a coordinate singularity in the real part of η. For this reason we chose to instead calculate the boost angle using Kruskal coordinates, in which it is well-defined on the horizon. In order to produce some preliminary plots of the boost angle, we set the Schwarzschild radius $r_s = 1$ and chose values of $E_1 = -2$, $E_2 = 2$ for the conserved quantities associated to the maximal surfaces. The correct choice of values for E_1 and E_2 requires careful consideration; this is an area for future work that we discuss further in Chapter 7. The preliminary plots of the boost angle in Kruskal coordinates agree with the results we obtained using Schwarzschild coordinates. The real part of the boost angle is suppressed in the majority of the interior region of the black hole ($r < r_s$), and increases to a finite maximum near the horizon at $r = r_s$. Similarly for the exterior of the black hole $r > r_s$, the real part of η is suppressed in most of the exterior region and increases as we approach the horizon. The imaginary part of η is zero in the interior, and has a constant value of $i\pi$ in the exterior. As previously mentioned, we require the boost angle to have a finite imaginary part in the region of spacetime in which the tunnelling transition takes place. On the horizon $r = r_s$, we found that the boost angle reduces to $\eta = i\pi$ for our chosen values of the conserved quantities $E_1 = -2$ and $E_2 = 2$, i.e. it is purely imaginary. Comparison with the plots of η for the interior and exterior regions of the black hole suggests that for the values that we chose, the boost angle is not continuous across the horizon as we expect it to be in the Kruskal coordinates. This indicates that $E_1 = -2$ and $E_2 = 2$ may not be suitable choices for the conserved quantities.

Chapter 7

Concluding Remarks & Future Work

In this thesis we investigated the proposal that near the end of its evaporation, a black hole will not simply disappear but will instead undergo a quantum transition into a white hole. This transition takes the form of quantum tunnelling. We chose to study a Schwarzschild black hole, and define the region in which quantum effects dominate as enclosed by intersecting hypersurfaces on which the trace of the extrinsic curvature is equal to zero. We found that the gravitational action for this spacetime is dependent only on the action term at the corner of the quantum gravity region, and the corner action is determined by the boost angle between the normal vectors to the two intersecting hypersurfaces (maximal surfaces). Using Kruskal coordinates, we deduced an expression for the boost angle dependent on how the maximal surfaces are defined. Our results indicate that the real part of the boost angle increases from each direction (both from the exterior and interior regions of the black hole) and reaches a finite maximum value close to the horizon. This makes intuitive sense; since the tunnelling probability is dependent on the value of the boost angle and we assume that the quantum transition will occur near the horizon, we expect the angle to increase as we approach the horizon. The boost angle is zero inside the horizon, and has a constant imaginary part in the exterior region. A constant imaginary part in the boost angle is required in order for tunnelling to occur. Upon simplifying our expression for the boost angle on the horizon, we found that the real part of the boost angle appears to be discontinuous across the horizon, which does not match our expectations. However, the apparent discontinuity in the boost angle across the horizon could be a consequence of an unsuitable choice for the values of the conserved quantities associated to the maximal surfaces.

The characterization of the maximal surfaces is something that we would like to improve our understanding of. We chose to define the quantum gravity region as enclosed by the intersecting maximal surfaces on which the trace of the extrinsic curvature is zero. We are as yet unsure of the location of the corner of the quantum gravity region, $\mathcal{J}$. The corner could be located either just inside, just outside or directly on the horizon; at present we have no sufficient reason to impose the location at any of these points. A useful first step in understanding the quantum gravity region better could be to locate the corner by numerically solving the differential equations defining the maximal surfaces (Equation

6.14). On the black hole horizon, we found that the boost angle is independent of the spacetime coordinates R and T, and depends only on the conserved quantities E_1 and E_2 that characterize the maximal surfaces. E_1 and E_2 are clearly critical in the calculation of the boost angle, so it is important that we understand how to choose their values correctly. We would like to understand what the allowed values of E_1 and E_2 are for a given value of r_s.

We note that there are several limitations to our study, one of which being the fact that we have used a static approximation to model the black hole to white hole transition. This approximation is only valid if the time taken for the quantum transition is very small compared to the time taken for the black hole to evaporate via Hawking radiation (and the time taken for matter to leak out from the white hole). We have not considered the relative timescales for these processes in this study. Additionally, this work does not offer any insight into the solution to the information loss problem. We have not considered what happens to the information trapped inside a black hole during Hawking evaporation, or proposed any mechanism by which the information inside the black hole can escape after the quantum tunnelling transition to a white hole occurs.

7.1 The Complex Solution of Einstein's Equations

We now consider a less immediate area for future study, and a way in which we could extend our current work. In order to deduce an expression for the probability that a Planck-mass black hole will quantum tunnel into a white hole we have focused our analysis on the tunnelling region B (see Section 1.1.3), where the trapping black hole horizon evolves into an anti-trapping white hole horizon. However, to obtain a complete picture of black hole to white hole quantum tunnelling we must also take the high curvature region (Region A) into consideration. It is necessary to show that there is a complex solution to the Einstein equations that extends across the Schwarzschild singularity at $r = 0$. For this purpose, we consider a Schwarzschild solution first proposed by Synge in 1950 [82]. We first note that the interior of a Schwarzschild black hole can be foliated by spacelike surfaces that are three-dimensional cylinders, i.e. $S^2 \times \mathbb{R}$. The line element in each of these cylinders is given by

$$\mathrm{d}s^2 = -\frac{4\tau^4}{2m-\tau^2}\mathrm{d}\tau^2 + \frac{2m-\tau^2}{\tau^2}\mathrm{d}x^2 + \tau^4\mathrm{d}\Omega^2 \tag{7.1}$$

where τ is a temporal coordinate and x is a spatial coordinate running along a portion of the cylinder's axis. If we let $\tau < 0$ and choose the Schwarzschild coordinates

$$t = x \tag{7.2a}$$

$$r = \tau^2, \tag{7.2b}$$

we find

$$\mathrm{d}s^2 = -\left(1-\frac{2m}{r_s}\right)\mathrm{d}t^2 + \left(1-\frac{2m}{r_s}\right)^{-1}\mathrm{d}r^2 + r_s^2\mathrm{d}\Omega^2 \tag{7.3}$$

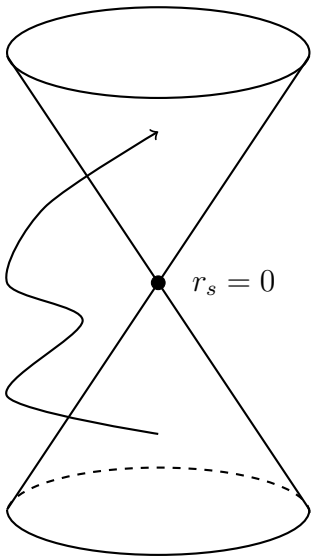

Figure 7.1: A visual representation of Synge's solution for the continuation of the Schwarzschild line element across the singularity at $r_s = 0$. The bottom half of the diagram is the interior geometry of the black hole, and the top half is the interior geometry of the white hole that it tunnels into. The arrow indicates how the singularity may be circumvented by allowing the temporal coordinate τ to move to the complex plane.

which is the line element describing the interior of a Schwarzschild black hole. If we instead choose $\tau > 0$, Equation 7.3 describes the interior of a white hole. We can therefore view Synge's solution (Equation 7.1) as the natural extension of a black hole's interior geometry across the Schwarzschild singularity, and into the interior of a white hole.

Although Synge's solution succeeds in describing the continuation of a black hole's interior geometry into that of a white hole, the method by which we avoid the central singularity is as yet unexplained. Consider the discussion in Appendix A concerning the semiclassical description of time-dependent quantum tunnelling. We show that allowing time paths to move to the complex plane enables us to use semiclassical VVG theory to model barrier tunnelling. We now propose to apply the same logic to Synge's theory: complexification of the temporal coordinate τ will result in a complex Schwarzschild solution which satisfies the Einstein equations exactly throughout the whole of the quantum gravity region. Complexification of the Synge solution allows a gluing of 'complex gravity' everywhere from the black hole horizon to the white hole horizon.

Figure 7.1 is a visual representation of the complex Synge solution described above. The bottom half of the diagram represents the interior geometry of an old black hole, and the top half is the interior geometry of a white hole. The black hole would ordinarily need to cross the central singularity at $r_s = 0$ in order to complete the quantum transition into a white hole. However, if we allow the temporal coordinate τ in the Synge solution to move to the complex plane, the Schwarzschild singularity can be circumvented (as shown by the arrow).

The ideas presented in this section are preliminary, and require a great deal of mathe-

matical development. Time constraints have thus far prevented us from further exploration of the complex Synge solution, but we believe it is a promising area for future study. In order to show that we can use the complex Synge solution to describe black hole to white hole quantum tunnelling, we must reformulate Einstein's general relativity in terms of complex variables. The first step in this process is to complexify the coordinates of the spacetime metric.

References

[1] Emanuele Alesci, Sina Bahrami, and Daniele Pranzetti. Quantum evolution of black hole initial data sets: Foundations. *Physical Review D*, 98(4):046014, 2018.

[2] Emanuele Alesci, Sina Bahrami, and Daniele Pranzetti. Quantum gravity predictions for black hole interior geometry. *arXiv preprint arXiv:1904.12412*, 2019.

[3] Matthew Ambrose. Path integral formulation of quantum tunneling: Numerical approximation and application to coupled domain wall pinning.

[4] Marcel Ambrus and P Hájíček. Quantum superposition principle and gravitational collapse: Scattering times for spherical shells. *Physical Review D*, 72(6):064025, 2005.

[5] Joachim Ankerhold and Markus Saltzer. Semiclassical wave packet tunneling in real-time. *Physics Letters A*, 305(5):251–257, 2002.

[6] Abhay Ashtekar, Alejandro Corichi, and Parampreet Singh. Robustness of key features of loop quantum cosmology. *Physical Review D*, 77(2):024046, 2008.

[7] Abhay Ashtekar, Javier Olmedo, and Parampreet Singh. Quantum extension of the kruskal spacetime. *Physical Review D*, 98(12):126003, 2018.

[8] Abhay Ashtekar, Javier Olmedo, and Parampreet Singh. Quantum transfiguration of kruskal black holes. *Physical review letters*, 121(24):241301, 2018.

[9] Abhay Ashtekar, Tomasz Pawlowski, and Parampreet Singh. Quantum nature of the big bang: improved dynamics. *Physical Review D*, 74(8):084003, 2006.

[10] James M Bardeen. Black hole evaporation without an event horizon. *arXiv preprint arXiv:1406.4098*, 2014.

[11] Aurélien Barrau, Killian Martineau, and Flora Moulin. A status report on the phenomenology of black holes in loop quantum gravity: Evaporation, tunneling to white holes, dark matter and gravitational waves. *Universe*, 4(10):102, 2018.

[12] Aurélien Barrau, Carlo Rovelli, and Francesca Vidotto. Fast radio bursts and white hole signals. *Physical Review D*, 90(12):127503, 2014.

[13] Eugenio Bianchi, Marios Christodoulou, Fabio D'Ambrosio, Hal M Haggard, and Carlo Rovelli. White holes as remnants: A surprising scenario for the end of a black hole. *Classical and Quantum Gravity*, 35(22):225003, 2018.

[14] Léon Brillouin. The wave mechanics of schrödinger: a general method of solving the problem by successive approximations. *Compt. Makes. Hebd. Acadian Sessions Sci.*, 183:24–26, 1926.

[15] Sean M Carroll. *Spacetime and geometry. An introduction to general relativity*, chapter 5, page 193. 2004.

[16] Sean M Carroll. *Spacetime and geometry. An introduction to general relativity*, chapter 6, page 244. 2004.

[17] Sean M Carroll. *Spacetime and geometry. An introduction to general relativity*, chapter 5, page 224. 2004.

[18] Sean M Carroll. *Spacetime and geometry. An introduction to general relativity*. 2004.

[19] Sean M Carroll. *Spacetime and geometry. An introduction to general relativity*, chapter 5, page 204. 2004.

[20] Masud Chaichian and Andrei Demichev. *Path integrals in physics: Volume I stochastic processes and quantum mechanics*, page 1. CRC Press, 2001.

[21] Masud Chaichian and Andrei Demichev. *Path integrals in physics: Volume I stochastic processes and quantum mechanics*. CRC Press, 2001.

[22] Marios Christodoulou and Fabio D'Ambrosio. Characteristic time scales for the geometry transition of a black hole to a white hole from spinfoams. *arXiv preprint arXiv:1801.03027*, 2018.

[23] Marios Christodoulou and Tommaso De Lorenzo. Volume inside old black holes. *Physical Review D*, 94(10):104002, 2016.

[24] Marios Christodoulou and Carlo Rovelli. How big is a black hole? *Physical Review D*, 91(6):064046, 2015.

[25] Marios Christodoulou, Carlo Rovelli, Simone Speziale, and Ilya Vilensky. Planck star tunneling time: An astrophysically relevant observable from background-free quantum gravity. *Physical Review D*, 94(8):084035, 2016.

[26] Robert M Corless, Gaston H Gonnet, David EG Hare, David J Jeffrey, and Donald E Knuth. On the lambertw function. *Advances in Computational mathematics*, 5(1):329–359, 1996.

[27] Predrag Cvitanovic, Roberto Artuso, Ronnie Mainieri, Gregor Tanner, Gábor Vattay, Niall Whelan, and Andreas Wirzba. *Chaos: classical and quantum*, volume 69, chapter 38, page 691. 2005.

[28] Tommaso De Lorenzo and Alejandro Perez. Improved black hole fireworks: Asymmetric black-hole-to-white-hole tunneling scenario. *Physical Review D*, 93(12):124018, 2016.

[29] Paul AM Dirac. The lagrangian in quantum mechanics. In *Feynman's Thesis—A New Approach To Quantum Theory*, pages 111–119. World Scientific, 2005.

[30] JD Doll, TF George, and WH Miller. Complex-valued classical trajectories for reactive tunneling in three-dimensional collisions of h and h2. *The Journal of Chemical Physics*, 58(4):1343–1351, 1973.

[31] Richard Phillips Feynman. Space-time approach to non-relativistic quantum mechanics. In *Feynman's Thesis—A New Approach To Quantum Theory*, pages 71–109. World Scientific, 2005.

[32] RP Feynman. The principle of least action in quantum mechanics (princeton university, ann arbor, 1942; university microfilms publication no. 2948). rp feynman. *Rev. Mod. Phys*, 20:367, 1948.

[33] RP Feynman and AR Hibbs. Path integrals and quantum mechanics. *McGraw, New York*, 1965.

[34] Valeri P Frolov. Information loss problem and a 'black hole'model with a closed apparent horizon. *Journal of High Energy Physics*, 2014(5):49, 2014.

[35] Valeri P Frolov and GA Vilkovisky. Quantum gravity removes classical singularities and shortens the life of black holes. Technical report, International Centre for Theoretical Physics, 1979.

[36] Valeri P Frolov and GA Vilkovisky. Spherically symmetric collapse in quantum gravity. In *Quantum Gravity*, pages 267–290. Springer, 1984.

[37] G Gamow. Quantum theory of the atomic nucleus. *Z. Phys. A*, 51, 01 1928.

[38] George Gamow. The quantum theory of nuclear disintegration. *Nature*, 122(3082):805, 1928.

[39] George Gamow. *Constitution of atomic nuclei and radioactivity*. Oxford, 1931.

[40] Steven B Giddings. Black holes and massive remnants. *Physical Review D*, 46(4):1347, 1992.

[41] Frank Grossmann and Eric J Heller. A semiclassical correlation function approach to barrier tunneling. *Chemical physics letters*, 241(1-2):45–50, 1995.

[42] Martin C Gutzwiller. Phase-integral approximation in momentum space and the bound states of an atom. *Journal of mathematical Physics*, 8(10):1979–2000, 1967.

[43] Martin C Gutzwiller. Phase-integral approximation in momentum space and the bound states of an atom. *J. Math. Phys.*, 8:1979, 1967.

[44] Martin C Gutzwiller. Chaos in classical and quantum mechanics, volume 1 of interdisciplinary applied mathematics, 1990.

[45] HM Haggard and C Rovelli. Black hole fireworks: quantum-gravity effects outside the horizon spark black to white hole tunneling, 2014. *arXiv preprint arXiv:1407.0989*.

[46] Petr Hájíček and Claus Kiefer. Singularity avoidance by collapsing shells in quantum gravity. *International Journal of Modern Physics D*, 10(06):775–779, 2001.

[47] Stephen Hawking and Roger Penrose. *The nature of space and time*. Princeton University Press, 2010.

[48] Stephen W Hawking and George Francis Rayner Ellis. *The large scale structure of space-time*, volume 1. Cambridge university press, 1973.

[49] Stephen William Hawking and CJ Hunter. The gravitational hamiltonian in the presence of non-orthogonal boundaries. *Classical and Quantum Gravity*, 13(10):2735, 1996.

[50] Geoff Hayward. Gravitational action for spacetimes with nonsmooth boundaries. *Physical Review D*, 47(8):3275, 1993.

[51] Sean A Hayward. Formation and evaporation of nonsingular black holes. *Physical review letters*, 96(3):031103, 2006.

[52] Barry R Holstein. *Topics in advanced quantum mechanics*, chapter 5. Courier Corporation, 2013.

[53] Sabine Hossenfelder, Leonardo Modesto, and Isabeau Prémont-Schwarz. Model for nonsingular black hole collapse and evaporation. *Physical Review D*, 81(4):044036, 2010.

[54] Ian Jubb, Joseph Samuel, Rafael D Sorkin, and Sumati Surya. Boundary and corner terms in the action for general relativity. *Classical and Quantum Gravity*, 34(6):065006, 2017.

[55] Kenneth G Kay. Time-dependent semiclassical tunneling through barriers. *Physical Review A*, 88(1):012122, 2013.

[56] Hendrik Anthony Kramers. Wave mechanics and half-integer quantization. *Journal of Physics*, 39(10-11):828–840, 1926.

[57] NT Maitra and EJ Heller. Barrier tunneling and reflection in the time and energy domains: The battle of the exponentials. *Physical review letters*, 78(16):3035, 1997.

[58] NT Maitra and EJ Heller. Classical, semiclassical and quantum dynamics in atoms. *Springer Lecture Notes in Physics, edited by H. Friedrich and B. Eckhardt Springer-Verlag, Berlin*, 1997.

[59] William H Miller. Classical-limit quantum mechanics and the theory of molecular collisions. *Advances in chemical physics*, pages 69–177, 1974.

[60] William H Miller. Semiclassical limit of quantum mechanical transition state theory for nonseparable systems. *The Journal of chemical physics*, 62(5):1899–1906, 1975.

[61] William H Miller and Thomas F George. Semiclassical theory of electronic transitions in low energy atomic and molecular collisions involving several nuclear degrees of freedom. *The Journal of Chemical Physics*, 56(11):5637–5652, 1972.

[62] Leonardo Modesto. Disappearance of the black hole singularity in loop quantum gravity. *Physical Review D*, 70(12):124009, 2004.

[63] JV Narlikar, KMV Appa Rao, and Naresh Dadhich. High energy radiation from white holes. *Nature*, 251(5476):590, 1974.

[64] Javier Olmedo, Sahil Saini, and Parampreet Singh. From black holes to white holes: a quantum gravitational, symmetric bounce. *Classical and Quantum Gravity*, 34(22):225011, 2017.

[65] Eric Poisson. *A relativist's toolkit: the mathematics of black-hole mechanics*. Cambridge university press, 2004.

[66] Eric Poisson. *A relativist's toolkit: the mathematics of black-hole mechanics*, chapter 5, page 164. Cambridge university press, 2004.

[67] Eric Poisson. *A relativist's toolkit: the mathematics of black-hole mechanics*, chapter 5, page 168. Cambridge university press, 2004.

[68] John Preskill. Do black holes destroy information. In *Proceedings of the International Symposium on Black Holes, Membranes, Wormholes and Superstrings, S. Kalara and DV Nanopoulos, eds.(World Scientific, Singapore, 1993) pp*, pages 22–39. World Scientific, 1992.

[69] Mohsen Razavy. *Quantum theory of tunneling*, chapter 1, page 1. World Scientific, 2003.

[70] Mohsen Razavy. *Quantum theory of tunneling*, chapter 1, page 2. World Scientific, 2003.

[71] Mohsen Razavy. *Quantum theory of tunneling*, chapter 2, page 9. World Scientific, 2003.

[72] Mohsen Razavy. *Quantum theory of tunneling*, chapter 13, page 285. World Scientific, 2003.

[73] Harvey Reall. Part 3 black holes, lecture notes given as part of the cambridge university mathematical tripos. 2014.

[74] Joel Robbin and Dietmar Salamon. The maslov index for paths. *Topology*, 32(4):827–844, 1993.

[75] Joel Robbin and Dietmar Salamon. Feynman path integrals on phase space and the metaplectic representation. *Mathematische Zeitschrift*, 221(1):307–335, 1996.

[76] Carlo Rovelli. Black hole evolution traced out with loop quantum gravity. *arXiv preprint arXiv:1901.04732*, 2019.

[77] Carlo Rovelli and Francesca Vidotto. Evidence for maximal acceleration and singularity resolution in covariant loop quantum gravity. *Physical review letters*, 111(9):091303, 2013.

[78] Carlo Rovelli and Francesca Vidotto. Planck stars. *International Journal of Modern Physics D*, 23(12):1442026, 2014.

[79] Markus Saltzer and Joachim Ankerhold. Semiclassical tunneling in real time: Wave-packet dynamics in static and driven barrier potentials. *Physical Review A*, 68(4):042108, 2003.

[80] Akira Shudo and Kensuke S Ikeda. Complex classical trajectories and chaotic tunneling. *Physical review letters*, 74(5):682, 1995.

[81] Akira Shudo and Kensuke S Ikeda. Chaotic tunneling: A remarkable manifestation of complex classical dynamics in non-integrable quantum phenomena. *Physica D: Nonlinear Phenomena*, 115(3-4):234–292, 1998.

[82] John Lighton Synge. The gravitational field of a particle. In *Proceedings of the Royal Irish Academy. Section A: Mathematical and Physical Sciences*, pages 83–114. JSTOR, 1950.

[83] John H Van Vleck. The correspondence principle in the statistical interpretation of quantum mechanics. *Proceedings of the National Academy of Sciences of the United States of America*, 14(2):178, 1928.

[84] Jiri Vanicek. Uniform semiclassical methods and their applications. 2003.

[85] Thomas W. Baumgarte and Stuart L. Shapiro. Numerical relativity: Solving einstein's equations on the computer. *Physics Today*, 64, 02 2011.

[86] Gregory Wentzel. A generalization of the quantum conditions for the purposes of wave mechanics. *Journal of Physics*, 38(6-7):518–529, 1926.

[87] Norbert Wiener. The average of an analytic functional and the brownian movement. *Proceedings of the National Academy of Sciences of the United States of America*, 7(10):294, 1921.

[88] Alec Yonika, Gaurav Khanna, and Parampreet Singh. von-neumann stability and singularity resolution in loop quantized schwarzschild black hole. *Classical and Quantum Gravity*, 35(4):045007, 2018.

[89] John ZH Zhang. New method in time-dependent quantum scattering theory: Integrating the wave function in the interaction picture. *The Journal of chemical physics*, 92(1):324–331, 1990.

Appendices

Appendix A

Time-Dependent Semiclassical Tunnelling Through Barriers

We consider the semiclassical theory of Van Vleck and Gutzwiller, and whether we can use this theory to describe quantum tunnelling through a potential barrier. We begin by reviewing the results of Kenneth Kay's paper 'Time-dependent semiclassical tunnelling through barriers' [55]. Kay addresses the question of whether semiclassical VVG theory can be used to describe time-dependent barrier tunnelling. He concludes that we may indeed use VVG theory to model barrier tunnelling, with the caveat that classical trajectories with both complex initial conditions and complex time paths must be taken into consideration. As a simple example, Kay applies this technique to the propagation of a particle through a classically forbidden one-dimensional barrier; a problem for which it would be impossible to create a model using VVG theory without the consideration of complex time.

A.1 Semiclassical VVG Theory & Time-Dependent Tunnelling

The 'semiclassical' or 'short-wavelength' approximation to quantum mechanics arises when we take the limit $\hbar \to 0$ in quantum mechanics in order to recover the results of classical physics [84]. Semiclassical physics has been in existence since the advent of quantum theory: before the derivation of Schrödinger's equation, Bohr had used the quantization condition

$$\oint p dq = 2\pi\hbar n \tag{A.1}$$

to describe the hydrogen spectrum. This condition selects classical states whose action is an integer multiple of $2\pi\hbar = h$. It was shown by Wentzel, Kramers and Brillouin that if we make a small adjustment to the integer n (dependent on the motion of the system), Bohr's quantization condition can be recovered from the time-independent Schrödinger equation in the short-wavelength limit [14, 56, 86]. This approximation, referred to as the 'WKB approximation', may be used to describe the tunnelling of a particle through a one-dimensional potential barrier.

Almost simultaneously with the development of WKB theory, the first semiclassical form of the quantum propagator was proposed by Van Vleck [83]. Consider a one-dimensional system with a particle that is initially at position x at time $t = 0$. It tunnels through a potential barrier and reaches its final position x at time $t = T$. The propagator $K(x', x, t) = \langle x' | \exp\Big(-i\hat{H}t/\hbar\Big) | x \rangle$ can be expressed as

$$K(x', x, t) = \sum_{\text{traj}} [D/(2\pi i\hbar)]^{1/2} e^{iS(x',x,t)/\hbar - i\pi\nu/2} \tag{A.2}$$

where $D = |\partial^2 S/\partial x' \partial x|$, and the sum is over all possible trajectories of the particle. The action $S(x', x, t)$ along a path is defined by

$$S(x, x', t) = \int_0^t [p(\tau)\dot{q}(\tau) - H(q(\tau), p(\tau))] d\tau \tag{A.3}$$

where H is the Hamiltonian, and q and p are position and momentum of the particle respectively. The Morse index ν is the number of times that the value of D on a particular path is infinite. The original Van Vleck propagator was written without the phase $\pi\nu/2$; this term was added later by Gutzwiller [42]. We therefore refer to Equation A.2 as the VVG propagator. Similar to the WKB approximation, VVG theory is a short-wavelength approximation to quantum mechanics. However, unlike WKB theory, the VVG propagator can be generalized to higher dimensions [27]. It can be derived directly from the Feynman propagator, if we use the stationary phase method to evaluate the integral. The stationary phase method is necessary because it selects only the classically allowed trajectories. It was not immediately obvious if it was possible to use semiclassical VVG theory to describe time-dependent quantum tunnelling. Kay addresses this question, and concludes that we may use VVG theory to describe time-dependent barrier tunnelling if we allow the particle to follow complex time paths with complex initial conditions.

A.2 Complex Energy & Time

We denote the energy of the particle by E, and the height of the potential barrier by V_0. The initial position x is on the left side of the barrier, and the final position x' is on the right. There are two separate scenarios to be considered:

- Case 1: $E < V_0$

  If the energy of the particle is greater than the height of the barrier, the time taken for the particle to travel from x to x' is real, and thus the action $S(x', x, t)$ is also real.

- Case 2: $E > V_0$

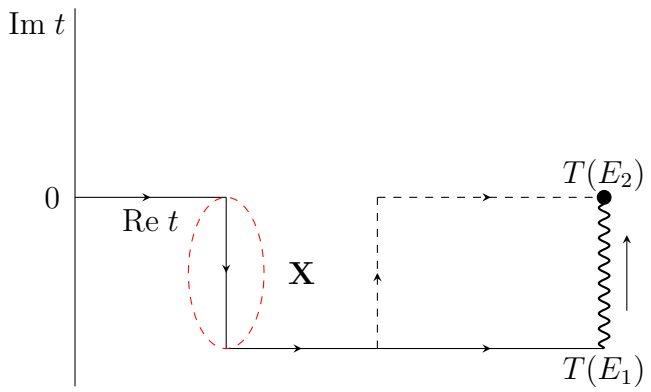

Figure A.1: Solid lines represent a typical WKB path from $t = 0$ to $t = T(E_1)$ for a real energy E_1, which circumvents the singularity at **X**. The final time can become real if we allow energy to change to a complex value E_2. The dashed black lines show an alternate complex time path. The dashed red lines indicate the region in which quantum tunnelling takes place.

> If the particle's energy is less than the barrier height, there is no real time path that it can take. If we are to use semiclassical VVG theory to describe the tunnelling of the particle, we must allow the time path to move to the complex plane.

Figure A.1 shows how a time path that is real-valued at the initial and final points circumvents a singularity **X** by moving to the complex plane at an intermediate point along the path. The particle is at initial position x at time $t = 0$. Time advances in the real direction until the particle reaches the barrier, where the time path is then allowed to move to the complex plane. This movement in the negative imaginary direction can be viewed as the tunnelling of the particle through the barrier. The region in which the tunnelling occurs is indicated by the dashed red line in Figure A.1. During the barrier crossing, the position of the particle remains real but its momentum becomes imaginary. After the barrier has been crossed, time can again advance along the real axis until the particle reaches its final position x' at time $T(E_1)$. This time path, shown by the solid lines in Figure A.1, represents a typical WKB path for a particle with real energy E_1. The path is composed of three segments: a real segment as the particle approaches the potential barrier, the complex segment during which it tunnels through the barrier and the final real segment on the other side. The total time taken for the particle to travel from x to x' is therefore complex, which means that the total action is also complex. It is clear from Figure A.1 that $T(E_1)$, the time at which the particle reaches x', is imaginary. In order to obtain a real value for the final time, we allow the energy of the particle to take a complex value E_2, such that the final time is $T(E_2)$. The path from $t = 0$ to $t = T(E_2)$ is not unique; the dashed black line shows an alternative path with the same final time $T(E_2)$. Either of these paths will result in the avoidance of the branch point **X**, which is a singularity of the classical position and momentum variables in the complex plane.

A.3 Recovering the VVG Expression

In order to show that it is valid to use VVG theory to describe time-dependent tunnelling, it is useful to try to recover the VVG expression (Equation A.2) from the time-dependent propagator. The time-dependent propagator $K(x', x, t)$ may be written in terms of the energy-dependent Green's function $G(x', x, E) = \langle x'|(E - \hat{H})^{-1})|x\rangle$ as

$$K(x', x, t) = \frac{i}{2\pi} \int \exp(-iEt/\hbar) G(x', x, E) dE. \tag{A.4}$$

According to Gutzwiller [43, 44], for a system with one degree of freedom we may express $G(x', x, E)$ as

$$G(x', x, E) = \frac{1}{i\hbar} \sum_{\text{traj}} \frac{\exp[iW(x', x, E)/\hbar - i\pi\mu/2]}{|\dot{q}(T)\dot{q}(0)|^{1/2}}, \tag{A.5}$$

where the sum is over particle trajectories with energy E, initial position x and final position x'. $\dot{q}(0)$ and $\dot{q}(T)$ are the initial and final velocities of the particle, where $T = T(x', x, E)$ is the time along the path. μ is the Maslov index [74, 75]. W is the action,

$$W(x', x, E) = \int_x^{x'} p(q, E) dq, \tag{A.6}$$

where $p(q, E)$ is the momentum at position q and energy E. Alternatively we may parameterize the action by the time t along the path, such that

$$W(x', x, E) = \int_0^T p(q(t), E)\dot{q}(q(t), E) dt. \tag{A.7}$$

Substituting Equation A.5 into Equation A.4 and using the stationary phase method to evaluate the integral results in

$$K(x', x, t) = \sum_{\text{traj}} \frac{1}{2\pi\hbar} \int \frac{\exp(i\phi/\hbar - i\pi\mu/2)}{|\dot{q}(T)\dot{q}(0)|^{1/2}} dE, \tag{A.8}$$

where $\phi = -Et + W(x', x, E)$. Differentiating ϕ with respect to E gives

$$\begin{aligned} \frac{\partial\phi}{\partial E} &= -t + \frac{\partial W(x', x, E)}{\partial E} \\ &= -t + T(x', x, E) \end{aligned} \tag{A.9}$$

where the last line follows from the fact that $\partial W(x', x, E)/\partial E = T(x', x, E)$, the total time along the particle's trajectory. The points of stationary phase are therefore energies E_c that satisfy $T(x', x, E_c) = t$. Using known relations between the derivatives of W and S [44] and the fact that $S(x'x, t) = W(x', x, E_c) - E_c t$, we find that the VVG propagator (Equation A.2) is recovered from the time-dependent propagator (Equation A.4).

A.4 Special Case: The Eckart Potential

We know that the complex time paths used to determine trajectories should circumvent particular singularities t_*. But how can we locate these singularities? For a general one-dimensional potential energy function $V(q)$, the singularity times are given by

$$t_* = \int_x^{q_*} \frac{dq}{\dot{q}} \tag{A.10}$$

where the integral is evaluated along a complex path from x to a point q_*. Numerical techniques are usually required to perform this integral, but we find an exception in the Eckart potential.

The Eckart potential is given by

$$V(q) = V_0 \, \mathrm{sech}^2(q/a). \tag{A.11}$$

There exists an analytical expression [30] for the singularity times of this potential:

$$t_*(\pm, k) = \frac{a}{v}\left[-\tanh^{-1}\left(\frac{p}{mv}\coth(x/a)\right) \right.$$
$$\left. \pm \tanh^{-1}[(E/V_0)^{1/2}] + i\pi(k+1/2)\right] \tag{A.12}$$

where $p = \{2m[(E - V(x)]\}^{1/2}$ is the value of momentum for the trajectory at the initial point x, $v \equiv (2E/m)^{1/2}$, and $k = 0, \pm 1, \pm 2, \ldots$. From Equation A.12 it is clear that for the Eckart potential, there are two infinite series of singularities corresponding to the positive and negative signs. The singularity time relevant for the dominant tunnelling process is $t_*(+, -1)$.

To calculate a complex trajectory contributing to $K(x', x, t)$ for the Eckart potential, we first make a guess for the complex initial momentum $p(0)$. Application of Equation A.12 with $p = p(0)$ results in a complex time path that passes between the singularities described above. The classical equations of motion $\partial q(t)/\partial p(0)$ and $\partial p(t)/\partial p(0)$ are then integrated along this time path and the Newton-Raphson equation,

$$p_{new}(0) = p(0) + \frac{x' - q(t)}{\partial q(t)/\partial p(0)}, \tag{A.13}$$

is used to refine the estimate for the initial momentum. Iteration of this process gives a converged complex trajectory which satisfies the required boundary conditions.

A.5 Tunnelling Probability

We can show that this approach successfully describes quantum tunnelling by choosing a representation for the time-dependent propagator and recovering the WKB tunnelling probability

$$P(E) = e^{-2\theta(E)/\hbar} \tag{A.14}$$

where $\theta(E)$ is the WKB barrier penetration integral,

$$\theta(E) = \int_{x_<}^{x_>} \sqrt{2m[V(q) - E]}\, dq. \tag{A.15}$$

$x_<$ and $x_>$ are the turning points of the particle's motion, at the beginning and end of the time period in which tunnelling occurs.

As an example, we could choose the initial position-final momentum representation of the propagator $\bar{K}(p', x, t) \equiv \langle p'| \exp\Big(-i\hat{H}t/\hbar\Big)|x\rangle$:

$$\bar{K}(p', x, t) = \sum_{\text{traj}} [\bar{D}/(2\pi i\hbar)]^{1/2} e^{i\bar{S}(p', x, t)/\hbar - i\pi\bar{\nu}/2}. \tag{A.16}$$

In the above expression, the tunnelling particle has initial position $q(0) = x$ and final momentum $p(t) = p'$. The action $\bar{S}(p', x, t) = -ip'q(t) + S(q(t), x, t)$, $\bar{D} = -|\partial^2\bar{S}/\partial p'\partial x|$, and $\bar{\nu}$ is the Morse phase. Tunnelling probabilities in the limits $x \to \infty$ and $t \to \infty$ for this propagator can be calculated using Zhang's expression [89]:

$$P(E) = 2\pi\hbar(p/p')|\bar{K}(p', x, t)|^2. \tag{A.17}$$

Using conservation of energy arguments, we find that there is only one tunnelling trajectory that contributes to Equation A.16 (for more detailed reasoning, see [55]). The action may be written as

$$\bar{S}(p', x, t) = -p'x' + W(x', x, E) - Et \tag{A.18}$$

where $W(x', x, E)$ is the usual WKB action, and the only complex term in $\bar{S}(p', x, t)$. Since Im $W = \theta(E)$ [55], we find that the tunnelling probability for this representation of the propagator is reduced to the WKB probability, $P(E) = e^{-2\theta(E)/\hbar}$.

Appendix B

Boost Angle on the Horizon in Kruskal Coordinates

For completeness, we include here the steps for simplifying the expression for the boost angle on the horizon in Kruskal coordinates (see Section 6.2.3). Considering the positive branch $T = +R$ and starting from Equation 6.39, we have

$$\begin{aligned}
\cosh\eta_K &= -4e^{-1}\left(\frac{R^2r_s^{10}-E_1^2e}{4E_1Rr_s^5}\right)\left(\frac{R^2r_s^{10}-E_2^2e}{4E_2Rr_s^5}\right)\\
&+\frac{4e^{-1}}{R^2}\left(\frac{E_1e}{2r_s^5}+\frac{R^2r_s^{10}-E_1^2e}{4E_1r_s^5}\right)\left(\frac{E_2e}{2r_s^5}+\frac{R^2r_s^{10}-E_2^2e}{4E_2r_s^5}\right)\\
&=-4e^{-1}\left(\frac{R^2r_s^{10}-E_1^2e}{4E_1Rr_s^5}\right)\left(\frac{R^2r_s^{10}-E_2^2e}{4E_2Rr_s^5}\right)\\
&+\frac{4e^{-1}}{R^2}\left\{\frac{E_1E_2e^2}{4r_s^{10}}+\left(\frac{R^2r_s^{10}-E_1^2e}{4E_1r_s^5}\right)\left(\frac{R^2r_s^{10}-E_2^2e}{4E_2r_s^5}\right)\right.\\
&\left.+\frac{E_2e}{2r_s^5}\left(\frac{R^2r_s^{10}-E_1^2e}{4E_1r_s^5}\right)+\frac{E_1e}{2r_s^5}\left(\frac{R^2r_s^{10}-E_2^2e}{4E_2r_s^5}\right)\right\}\\
&=-4e^{-1}\left(\frac{R^2r_s^{10}-E_1^2e}{4E_1Rr_s^5}\right)\left(\frac{R^2r_s^{10}-E_2^2e}{4E_2Rr_s^5}\right)\\
&+4e^{-1}\left\{\frac{E_1E_2e^2}{4r_s^{10}R^2}+\left(\frac{R^2r_s^{10}-E_1^2e}{4E_1Rr_s^5}\right)\left(\frac{R^2r_s^{10}-E_2^2e}{4E_2Rr_s^5}\right)\right.\\
&\left.+\frac{E_2e}{2r_s^5R^2}\left(\frac{R^2r_s^{10}-E_1^2e}{4E_1r_s^5}\right)+\frac{E_1e}{2r_s^5R^2}\left(\frac{R^2r_s^4-E_2^2e}{4E_2r_s^5}\right)\right\}
\end{aligned}$$

$$\begin{aligned}
\cosh\eta_K &= 4e^{-1}\left\{\frac{E_1E_2e^2}{4r_s^{10}R^2}+\frac{E_2e}{2r_s^5R^2}\left(\frac{R^2r_s^{10}-E_1^2e}{4E_1r_s^5}\right)+\frac{E_1e}{2r_s^5R^2}\left(\frac{R^2r_s^{10}-E_2^2e}{4E_2r_s^5}\right)\right\}\\
&= \frac{E_1E_2e}{r_s^{10}R^2}+\frac{2E_2}{r_s^5R^2}\left(\frac{R^2r_s^{10}-E_1^2e}{4E_1r_s^5}\right)+\frac{2E_1}{r_s^5R^2}\left(\frac{R^2r_s^{10}-E_2^2e}{4E_2r_s^5}\right)\\
&= \frac{E_1E_2e}{r_s^{10}R^2}+\frac{E_2(R^2r_s^{10}-E_1^2e)}{2E_1R^2r_s^{10}}+\frac{E_1(R^2r_s^{10}-E_2^2e)}{2E_2R^2r_s^{10}}\\
&= \frac{E_1E_2e}{r_s^{10}R^2}+\frac{E_2}{2E_1}-\frac{E_1E_2e}{2R^2r_s^{10}}+\frac{E_1}{2E_2}-\frac{E_1E_2e}{2R^2r_s^{10}}\\
&= \frac{1}{2}\left(\frac{E_1}{E_2}+\frac{E_2}{E_1}\right). \qquad \text{(B.1)}
\end{aligned}$$

For the negative branch $T=-R$, we instead choose the negative signs in Equation 6.34. This results in

$$\cosh\eta_K = -4e^{-1}\left(\frac{R^2r_s^{10}-E_1^2e}{4E_1Rr_s^5}\right)\left(\frac{R^2r_s^{10}-E_2^2e}{4E_2Rr_s^5}\right) \qquad \text{(B.2)}$$

$$+\frac{4e^{-1}}{R^2}\left(\frac{E_1e}{2r_s^5}+\frac{R^2r_s^{10}-E_1^2e)}{4E_1r_s^5}\right)\left(\frac{E_2e}{2r_s^5}+\frac{R^2r_s^{10}-E_2^2e}{4E_2r_s^5}\right) \qquad \text{(B.3)}$$

and the rest of the steps are identical to those for the positive branch $T=+R$. For both $T=+R$ and $T=-R$ we therefore obtain the same expression for $\cosh\eta_K$:

$$\cosh\eta_K = \frac{1}{2}\left(\frac{E_1}{E_2}+\frac{E_2}{E_1}\right). \qquad \text{(B.4)}$$

Appendix C

MATLAB Code used to produce Figures 6.3 - 6.5

```
%%%%%%%%%%%%%%%%%%%%%%%%%%%%%%%%%%%%%%%%%%%%%%%%%%%%%%%%%%%%%%%%%%%%%%%%%%%%%%%%
 % PLOTTING THE BOOST ANGLE IN KRUSKAL COORDINATES - INTERIOR
%%%%%%%%%%%%%%%%%%%%%%%%%%%%%%%%%%%%%%%%%%%%%%%%%%%%%%%%%%%%%%%%%%%%%%%%%%%%%%%%
clear all
close all
r_s = 1; % Schwarzschild radius
N = 1e3;
R = linspace(-2,2,N);
T = linspace(0,2,N);
[R_mesh,T_mesh] = meshgrid(R,T);
E1 = -2;
E2 = 2;

% pre-allocate values for cosh_eta and eta
cosh_eta = zeros(N);
eta = zeros(N);

for n = 1:N % loop over T
    for m = 1:N % loop over R

% impose boundary conditions for BH interior
        if T(n)^2 - R(m)^2 <= 0
        eta(n,m) = NaN + 1i*NaN;
        elseif T(n)^2 - R(m)^2 >= 1
        eta(n,m) = NaN + 1i*NaN;
        else

            % calculate r
```

```
            w0 = lambertw(0,(R(m)^2 - T(n)^2)/exp(1));
            r = r_s*(1 + w0);

            % calculate T_dot
            A1 = R(m)^2 - T(n)^2;
            B1 = (E1*exp(r/r_s)*R(m))/(r^3*r_s^2);
            C1 = (E1^2*exp(2*r/r_s))/(4*r^6*r_s^4) - ...
                 r_s^3*exp(r/r_s)*(T(n)^2)/(4*r^3);
            T1_dot = (-B1 + sqrt(B1^2 - 4*A1*C1))/(2*A1);


            A2 = R(m)^2 - T(n)^2;
            B2 = (E2*exp(r/r_s)*R(m))/(r^3*r_s^2);
            C2 = (E2^2*exp(2*r/r_s))/(4*r^6*r_s^4) - ...
                 r_s^3*exp(r/r_s)*(T(n)^2)/(4*r^3);
            T2_dot = (-B2 + sqrt(B2^2 - 4*A2*C2))/(2*A2);

            % calculate R_dot
            R1_dot = (1/T(n))*((E1*exp(r/r_s)/(2*r^3*r_s^2)) + ...
                R(m)*T1_dot);
            R2_dot = (1/T(n))*((E2*exp(r/r_s)/(2*r^3*r_s^2)) + ...
                R(m)*T2_dot);

            % calculate b1 and b2
            b1 = 4*r*exp(-r/r_s)*T1_dot;
            b2 = 4*r*exp(-r/r_s)*T2_dot;

            % calculate eta
            cosh_eta(n,m) = (1.0/(4*r_s^3)) * (b1*b2*r*exp(r/r_s))*...
                (1 - (R1_dot*R2_dot)/(T1_dot*T2_dot));
            eta(n,m) = acosh(cosh_eta(n,m));
        end
    end
end

 % manually remove divergences (numerical artifacts)
for k = 0:floor(N)
    for l = floor(0.7*k) + 5: N - floor(0.7*k) - 5
        if eta(N-k,l) >= 4
            eta(N-k,l) = 4;
        end
    end
end
```

```
eta(eta>30) = NaN;

% plot boost angle
figure(1) % real part, 3D
surf(R_mesh,T_mesh,real(eta),'EdgeColor','interp')
xlabel('$R$','interpreter','latex','fontsize',30)
ylabel('$T$','interpreter','latex','fontsize',30)
zlabel('$Re(\eta_K)$','interpreter','latex','fontsize',30)

figure(2) % real part, 2D
surf(R_mesh,T_mesh,real(eta),'EdgeColor','interp')
view(2) % 2-d view in the (R,T) plane
xlabel('$R$','interpreter','latex','fontsize',30)
ylabel('$T$','interpreter','latex','fontsize',30)
zlabel('$Re(\eta_K)$','interpreter','latex','fontsize',30)

figure(3) % imaginary part, 3D
surf(R_mesh,T_mesh,imag(eta),'EdgeColor','interp')
xlabel('$R$','interpreter','latex','fontsize',30)
ylabel('$T$','interpreter','latex','fontsize',30)
zlabel('$Im(\eta_K)$','interpreter','latex','fontsize',30)

figure(4) % imaginary part, 2D
surf(R_mesh,T_mesh,imag(eta),'EdgeColor','interp')
view(2) % 2-d view in the (R,T) plane
xlabel('$R$','interpreter','latex','fontsize',30)
ylabel('$T$','interpreter','latex','fontsize',30)
zlabel('$Im(\eta_K)$','interpreter','latex','fontsize',30)
```

Appendix D

MATLAB Code used to produce Figures 6.6 - 6.8

```
%%%%%%%%%%%%%%%%%%%%%%%%%%%%%%%%%%%%%%%%%%%%%%%%%%%%%%%%%%%%%%%%%%%%%%%%%%%%%%%%
 % PLOTTING THE BOOST ANGLE IN KRUSKAL COORDINATES - EXTERIOR
%%%%%%%%%%%%%%%%%%%%%%%%%%%%%%%%%%%%%%%%%%%%%%%%%%%%%%%%%%%%%%%%%%%%%%%%%%%%%%%%
clear all
close all
r_s = 1; % Schwarzschild radius
N = 1e3;
R = linspace(0,2,N);
T = linspace(-2,2,N);
[R_mesh,T_mesh] = meshgrid(R,T);
E1 = -2;
E2 = 2;

% pre-allocate values for cosh_eta and eta
cosh_eta = zeros(N);
eta = zeros(N);

for n = 1:N % loop over T
    for m = 1:N % loop over R

% impose boundary conditions for BH exterior
        if T(n)^2 - R(m)^2 >= -0.0001 % set to 0
         eta(n,m) = NaN + 1i*NaN;
        else

            % calculate r
            w0 = lambertw(0,(R(m)^2 - T(n)^2)/exp(1));
            r = r_s*(1 + w0);
```

```
            % calculate T_dot
            A1 = R(m)^2 - T(n)^2;
            B1 = (E1*exp(r/r_s)*R(m))/(r^3*r_s^2);
            C1 = (E1^2*exp(2*r/r_s))/(4*r^6*r_s^4) - ...
                ((r_s^3) * exp(r/r_s)*T(n)^2)/(4*r^3);
            T1_dot = (-B1 + sqrt(B1^2 - 4*A1*C1))/(2*A1);

            A2 = R(m)^2 - T(n)^2;
            B2 = (E2*exp(r/r_s)*R(m))/(r^3*r_s^2);
            C2 = (E2^2*exp(2*r/r_s))/(4*r^6*r_s^4) - ...
                ((r_s^3) * exp(r/r_s)*T(n)^2)/(4*r^3);
            T2_dot = (-B2 + sqrt(B2^2 - 4*A2*C2))/(2*A2);

            % calculate R_dot
            R1_dot = (1/T(n))*((E1*exp(r/r_s)/(2*r^3*r_s^2)) + ...
                R(m)*T1_dot);
            R2_dot = (1/T(n))*((E2*exp(r/r_s)/(2*r^3*r_s^2)) + ...
                R(m)*T2_dot);

            % calculate b1 and b2
            b1 = 4*r*exp(-r/r_s)*T1_dot;
            b2 = 4*r*exp(-r/r_s)*T2_dot;

            % calculate eta
            cosh_eta(n,m) = (1.0/(4*r_s^3)) * (b1*b2*r*exp(r/r_s))*...
                (1 - (R1_dot*R2_dot)/(T1_dot*T2_dot));
            eta(n,m) = acosh(cosh_eta(n,m));
        end
    end
end

eta(eta>30)=NaN;

% plot boost angle
figure(1) % real part, 3D
surf(R_mesh,T_mesh,real(eta),'EdgeColor','interp')
xlabel('$R$','interpreter','latex','fontsize',30)
ylabel('$T$','interpreter','latex','fontsize',30)
zlabel('$Re(\eta_K)$','interpreter','latex','fontsize',30)

figure(2) % real part, 2D
surf(R_mesh,T_mesh,real(eta),'EdgeColor','interp')
view(2) % 2-d view in the (R,T) plane
```

```
xlabel('$R$','interpreter','latex','fontsize',30)
ylabel('$T$','interpreter','latex','fontsize',30)
zlabel('$Re(\eta_K)$','interpreter','latex','fontsize',30)

figure(3) % imaginary part, 3D
surf(R_mesh,T_mesh,imag(eta),'EdgeColor','interp')
xlabel('$R$','interpreter','latex','fontsize',30)
ylabel('$T$','interpreter','latex','fontsize',30)
zlabel('$Im(\eta_K)$','interpreter','latex','fontsize',30)

figure(4) % imaginary part, 2D
surf(R_mesh,T_mesh,imag(eta),'EdgeColor','interp')
view(2) % 2-d view in the (R,T) plane
xlabel('$R$','interpreter','latex','fontsize',30)
ylabel('$T$','interpreter','latex','fontsize',30)
zlabel('$Im(\eta_K)$','interpreter','latex','fontsize',30)
```